Characterization of Iron $^{R}Py_2N_2$ Azamacrocyclic Complexes as Carbon-Carbon Coupling Catalysts

Jackson Bonnell

TEXAS CHRISTIAN UNIVERSITY
The Boller Review: Vol. 8 2024

ACKNOWLEDGMENTS

I would like to thank everyone who has played a role in making this honors thesis a reality, namely my honors committee, the TCU Department of Chemistry and Biochemistry, The John V. Roach Honors College, the College of Science and Engineering, and a few important people individually.

To Katie Smith, wow, this paper is finally done. You and I have trucked through this project for what feels like forever, and you were an amazing friend and mentor to me all the way through. We are both on our way out, and I know you'll be an amazing professor one day.

To Mark, Spencer, and everyone else taking this project on once I leave, thank you for the help in this last stretch of the project. I wouldn't have been able to get those last few data points without y'all's help. In you guys, Dr. Green has a great set of undergrads going forward, and I'm excited to see where you guys take it from here.

To Will Campa, thanks for being a great friend through these past few years. I'm so glad you joined the Green lab, though I'm still a bit peeved I had to share my hood with you. Our workspace was *always* cluttered, but we made it work. Our time as chemists is over; let's go get those MDs.

To the rest of the Green Group, thanks for all of the compounds I got off of you, but more importantly, thanks for the good vibes. I'll miss y'all.

Finally, to Dr. Green. From literally day one of college, you have pushed me to grow as a person, and I will be forever grateful for that. It started as just making me learn half-decent study habits for your General Chemistry I class, but once you invited me to join your lab, you helped shape me into who I am today. Even though I am not going into chemistry like you wanted me to, I will still be using the things I have learned from you every day of my life. Thank you.

TABLE OF CONTENTS

INTRODUCTION

I. Catalysis Overview

Catalysis is the process of taking an exergonic reaction and making the reaction less energy-intensive, ideally resulting in an increased rate of reaction and yield. It lowers the overall activation energy of the total reaction by fundamentally altering the mechanism (or singular steps) of the reaction. Metal ions are particularly adept at acting as catalysts and often function by breaking the singular high-energy step into several consecutive low-energy steps that yield the product (Figure 1).

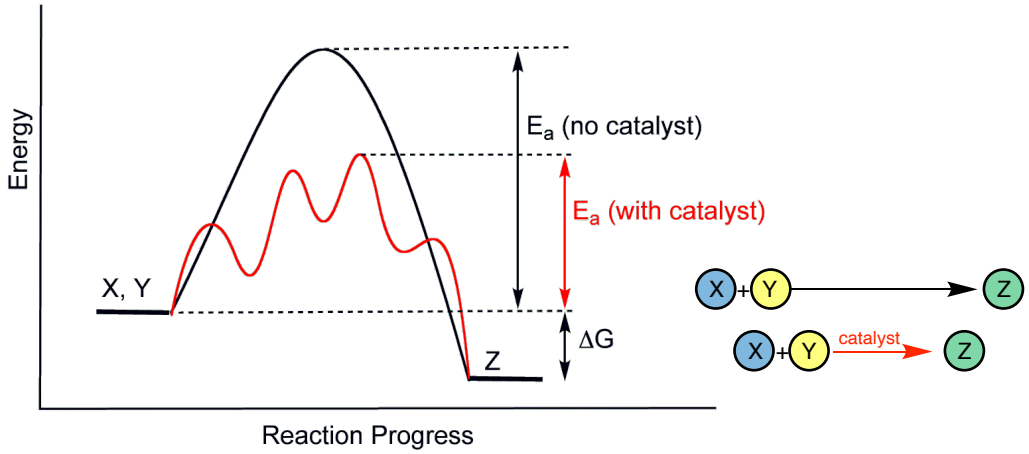

Figure 1. Catalysis energy diagram.[1]

Evidence of the importance of catalysis is all around us. More than 80% of all chemical products are produced with the aid of catalysis, accounting for over $900 billion annually in the United States economy. Products such as water bottles, paper, and gasoline are all made possible through catalysis (Figure 2).

Figure 2. Examples of catalytic products found in daily life. Left to right, top to bottom: plastic, gasoline, cheeses, paper, catalytic converters, Maillard products in pretzel crusts.

II. Carbon-Carbon Coupling Catalysis

A specific corner of the catalysis market is that of inorganic catalysis, crucial in the production of modern medicine, materials, fuels, and chemicals. The market for these catalysts runs in excess of $25 billion as of 2022 and is predicted to grow exponentially in coming years.[2]

In this project, I focused on the formation of carbon–carbon bonds, specifically C(sp^2)-C(sp^2) bonds, through the use of an inorganic catalyst. Most of these reactions reported to date make use of rare earth metal catalysts—notably, palladium—and are of extreme importance in industrial and medicinal applications. One pathway commonly used to form C-C bonds is termed Suzuki-Miyaura type coupling. This approach traditionally makes use of palladium catalysts to generate C-C bond formation between boronic acids/esters and a halide-activated arene (Scheme 1).

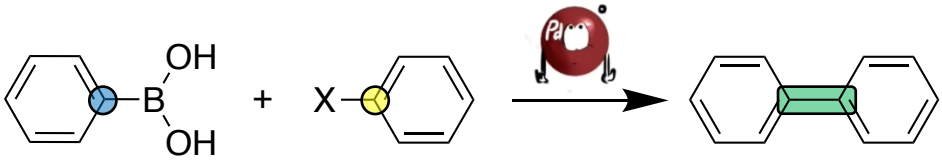

Scheme 1. Suzuki-Miyaura coupling general scheme.

The generally accepted mechanism for this reaction consists of three main steps: an oxidative addition, a transmetallation, and a reductive elimination.

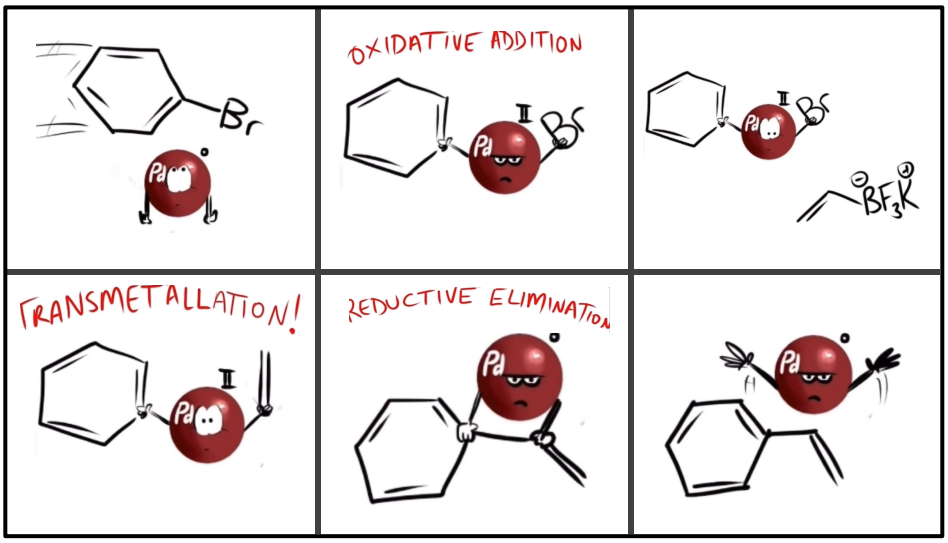

Figure 3. Suzuki-Miyaura Mechanism.[3]

The ubiquity of this reaction on the industrial scale can be exemplified by the large number of pharmaceuticals that engage Suzuki-Miyaura in the multi-step synthesis of heteroarenes, which are common architectures in natural products and/or pharmaceuticals. Examples of pharmaceuticals produced using this SM palladium-driven catalysis are: CI-1034, a vasodilator used to treat hypertensive patients; Norbadione A, a compound being investigated as a shield against irradiative damage; and Cytisine, an acetylcholine agonist used as an aid to quit smoking (Figure 4).

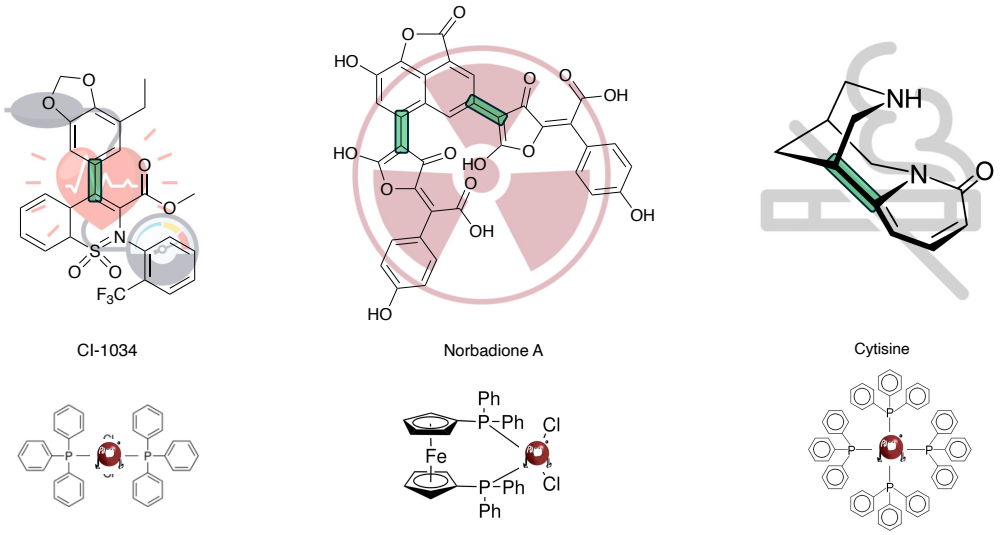

Figure 4. Organic structures of CI-1034, Norbadione A, and Cytisine. Highlighted bonds were formed through Suzuki-Miyaura coupling through the use of the palladium catalyst shown below the compound.[4]

III. Challenges with Palladium

While palladium has proven to be a highly effective catalyst for C-C coupling, it does present a number of challenges that are addressable using more contemporary approaches to catalysis. The following discussion will focus on detailing these challenges, and the overall goal of this project is to circumvent these challenges by using a different metal as the catalyst.

I. *Social Concerns Related to Palladium*

The acquisition of the palladium metal central to the success of these catalysts is surrounded by a host of issues. One such issue is the poor working conditions faced by the majority of the workers in this industry. In Rustenburg, South Africa, over 12,000 workers for one of the world's largest palladium suppliers, Anglo American Platinum, went on strike in 2012. Their list

of injustices included complaints about the lack of job security, the minimal safety training received, and the poor wages given in recompense for their brutal labor, amongst others. In the process of protesting, 34 of them were killed as a result of the local police attempting to quiet their voices. Even after this loss of life, the concerns were not addressed. Rather, each protestor was fired, ironically further establishing their protested lack of job security.[5]

II. *Environmental Concerns Related to Palladium*

The mines and refineries used to harvest and process palladium ore into a usable metal are extreme sources of pollution to the local environment. Mines utilize large volumes of the local water supply, the little left behind being polluted with heavy metals. The refineries have been recorded to produce more carbon dioxide and sulfur dioxide than an active volcano.[6] As such, palladium has a high global warming potential (GWP) of 3,880 kg CO_2/kg.[7]

III. *Health Concerns Related to Palladium*

The effects of this pollution are not just felt by the environment, but also the local populations. Norilsk is a city located in the largest palladium mining region of Russia. In this area, it is reported that the "snow that falls is black, the air smells of sulfur."[6] There are increased cases of respiratory, digestive, and nervous illnesses in children. Mothers experience more still and premature births than anywhere else in Russia. Cancer rates, especially cancers of the lungs, are at a much higher incidence. All of these and more contribute to the life expectancy in this region being 10 years below that of the Russian average, all in an effort to obtain palladium. Palladium itself is also more toxic than many elements. The International Council for the Harmonisation of Technical Requirements for Pharmaceuticals for Human Use (ICH) lists the permitted daily exposure (PDE) of palladium to be less than 100 μg per day.[8]

IV. *Cost Concerns Related to Palladium*.

Palladium is a rare earth metal, comprising less than 0.000002% of the Earth's crust. As a result of its scarcity and the issues in its acquisition, it is a costly metal to obtain. On its own, it is a costly element, costing $4,470/mol.[9] When including the ligand scaffolds around it, these catalysts grow even more expensive. The three catalyst examples shown in Figure 4, from left to right, cost $15,650/mol, $28,040/mol, and $18,260/mol, respectively, when purchased from Sigma Aldrich.

The costs associated with palladium usage have been known for years, and alternatives have been explored. Promising results have been found in the use of transition metal catalysts as

replacements for rare earth metal catalysts, especially in using iron-based catalysts to facilitate the coupling of $C(sp^2)$-$C(sp^2)$ bonds.

V. Benefits of Iron

Iron has been proposed as a potential substitute for palladium for years. As an abundant, non-toxic, and more sustainably mined element, iron faces none of these same issues as discussed with palladium.

I. Iron Acquisition

As an abundant earth metal, iron ore is found all over the world. Rather than rely on the production of the metal in countries like South Africa, with poorer working conditions, it is able to be more ethically sourced in mines from within the United States, where workers are protected by stringent safety standards and unions.

II. Environmental Impact of Iron Acquisition

As a result of its increased terrestrial availability and increased ease of refinement, iron has a much lower GWP than palladium, at 1.5 kg CO_2/kg, over 2,500 times less than that of palladium.[7]

III. Iron Associated Health Risks

As an essential element for human life, the risks associated with iron are minimal. The permitted daily exposure limit for iron is 60 mg/kg, drastically higher than that of palladium.[10]

IV. Cost of Iron

Iron is an earth-abundant metal, being the fourth most common element in the Earth's crust, comprising roughly 5.63% by mass. As such, it is an extremely cheap material, running for only $1/mol.[9] One of the ligands investigated herein, pyclen, can be synthesized in two steps, costing $5,800/mol, far beneath that of the comparable palladium complexes.

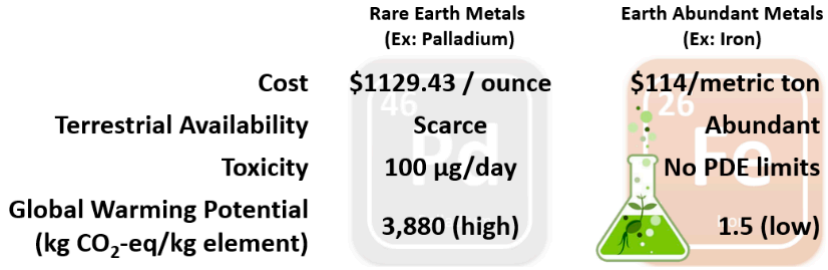

Figure 5. A side-by-side comparison of palladium and iron for their viability as catalytic centers.

Challenges with Aryl Halides. Another common reagent in these coupling reactions are aryl halides. These caustic halogenated compounds are used to direct the C-C bond formation and, ironically, also incorporate the use of palladium in their synthesis.

VI. Research Goals

In this work, I will investigate the ability of the Green Group's azamacrocyclic $^{R}Py_2N_2$ ligands to act as carbon-carbon coupling catalysts when complexed with iron with the goal of identifying iron-based catalysts that are competitive with the currently utilized palladium catalysts. The reaction investigated herein is the formation of 2-phenyl pyrrole as the result of the bond formation between pyrrole and phenylboronic acid (Scheme 2). This reaction also differs from Scheme 1 in that the biaryl product is the result of C-H bond functionalization of the pyrrole, rather than C-X functionalization previously shown, thus also eliminating the use of an aryl halide starting material.

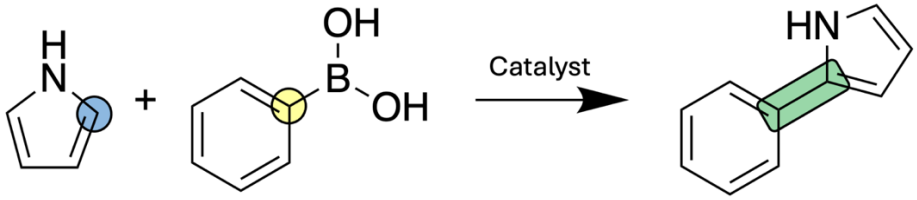

Scheme 2. 2-phenyl pyrrole synthesis by metal catalyzed bond formation between pyrrole and phenylboronic acid.

It has been found by Choy et al. (2018) that the coupling of pyrrole and phenylboronic acid can be run with yields up to 68% with the help of a palladium catalyst $Pd(TFA)_2$.[11] This palladium catalyst's performance will act as the 'benchmark' that we aim to meet herein.

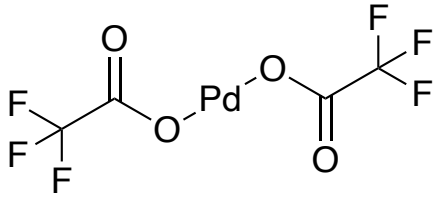

Figure 6. Structure of palladium (II) trifluoroacetate, $Pd(TFA)_2$.

It has previously been shown by Wen et al. (2010) that the formation of $C(sp^2)$-$C(sp^2)$ bonds (Scheme 2) can be facilitated by iron when complexed with cyclen-like ligands (Figure 7).

The group investigated the effects of the addition of pyridine and methyl moieties to the cyclen ring structure. These compounds were found to be able to catalyze the reaction with yields up to 81%, as determined by gas chromatography, and 68% yield isolated.[12]

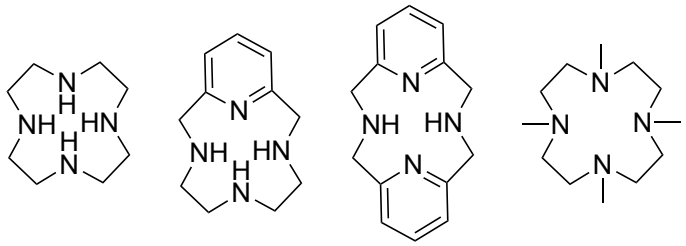

Figure 7. Cyclen-like ligands investigated by Wen et al. (2010) for iron-based C-C catalysis.

Inspired by the Wen Group, a previous member of the Green Group Dr. Magy Mekhail investigated our $^{R}\mathbf{PyN_3}$ series, a series of pyclen derivatives (Figure 8). These compounds were able to catalyze the reaction with yields ranging from 32-58% as determined by ^{1}H NMR, with substitution of electron withdrawing groups on the pyridine ring to provide the highest yields.[13]

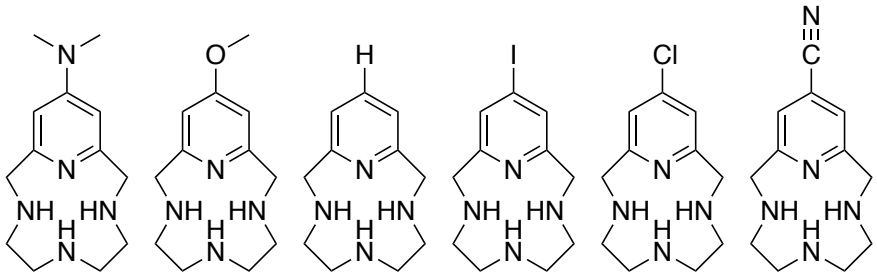

Figure 8. Para-substituted pyclen derivatives investigated by Mekhail et al. for iron-based C-C catalysis.

In this work, I will characterize the following library of ligands for their ability to catalyze this coupling reaction. This work was done in partnership with graduate student Katie Smith. **L1** was chosen in order to compare the results of this study to those of Wen et al. (2010) and Mekhail et al., and **L2**-**L5** were chosen for their range of electron-donating to electron-withdrawing substituents, as it was hypothesized that the strength of the metal chelating ability of the ring, characterized as a log β, would have an impact on the catalytic ability. **L6** was chosen to fit the range with **L2**-**L5** but was removed due to its ability to self-couple with the phenylboronic acid substrate.

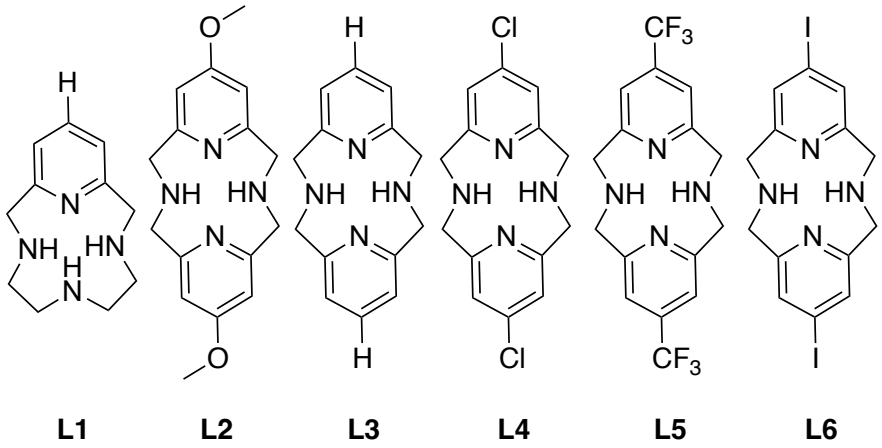

L1 **L2** **L3** **L4** **L5** **L6**

Figure 9. Ligand series **L1**-**L6** to be investigated herein.

RESULTS AND DISCUSSION

I. Synthetic Route: Ligands L1-L6

To determine the effects of para substitutions to the pyridine ring of these azamacrocycles on carbon coupling catalysis, ligands **L1** (^{H}**PyN$_3$**), **L2**, (^{OMe}**Py$_2$N$_2$**), **L3** (^{H}**Py$_2$N$_2$**), **L4** (^{Cl}**Py$_2$N$_2$**), **L5** (^{CF3}**Py$_2$N$_2$**), and **L6** (^{I}**Py$_2$N$_2$**) were synthesized according to the synthetic route displayed in Figure 10. **L2**, **L4**, **L5**, and **L6** share a common synthetic approach, being derived from their diester intermediates. **L1**, **L2**, and **L3** were obtained from lab mates David Freire (**L1**, **L3**), Sarah Dunn (**L4**), and Katie Smith (**L2**). Their synthetic methods are previously reported.[14,15]

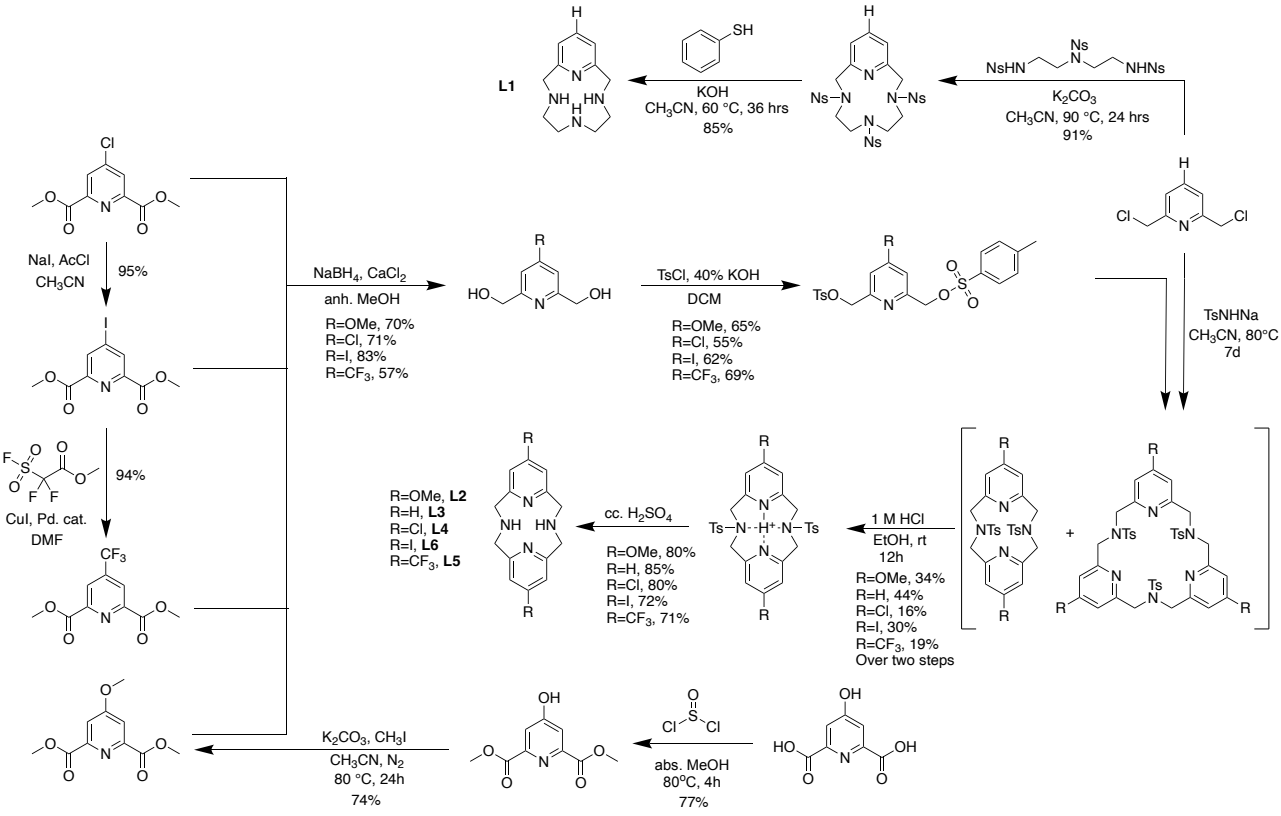

Figure 10. Synthetic scheme for **L1**-**L6**.

The **L2** ester (R = OMe) can be synthesized from chelidamic acid, which is subjected to an esterification by thionyl chloride in absolute methanol to provide a diester with a para hydroxy group with yields of 73%. This hydroxy group is then substituted with a methyl group through the addition of methyl iodide and potassium carbonate in acetonitrile in yields of 74%.

The **L4** ester (R = Cl) can be purchased directly and is purified through recrystallization in ethanol. The **L6** ester (R = I) can be synthesized from the **L4** ester, sonicating the ester in acetonitrile in the presence of acetyl chloride and sodium iodide to yield **L6** ester in yields of 88%. **L5** (R = CF_3) ester can be synthesized from the **L6** ester, refluxing it in dimethylformamide in the presence of copper (I) iodide, methyl 2,2-difluoro-2-(fluorosulfonyl)acetate, and (dppf)$PdCl_2$ • CH_2Cl_2 to provide **L5** ester in yields of 83%.

L2, **L4**, **L5**, and **L6** esters can be reduced to their respective diols through the addition of sodium borohydride and calcium chloride at room temperature in anhydrous methanol, in yields of 57-83%. **L2**, **L4**, **L5**, and **L6** diols can be tosylated by the addition of tosyl chloride and 40% KOH in DCM with yields of 55-69%. These tosylated products are then cyclized with sodium tosyl amide in acetonitrile to give a mixed product of desired 'dimer' and unwanted 'trimer.' To isolate the dimer, the mixture is washed with acidified ethanol, giving tosyl protected ^{R}**Py$_2$N$_2$** in yields of 16-34%. These are deprotected in concentrated sulfuric acid to give **L2**, **L4**, **L5**, and **L6** in yields of 71-85%. **L1-L6** ligands were characterized by ^{1}H NMR. Ligands with electron withdrawing groups (**L4-L6**) have aromatic resonances with downfield shifts compared to **L3**, and ligands with electron-donating groups (**L2**) have upfield shifted aromatic resonances.

II. Carbon-Carbon Coupling Catalysis

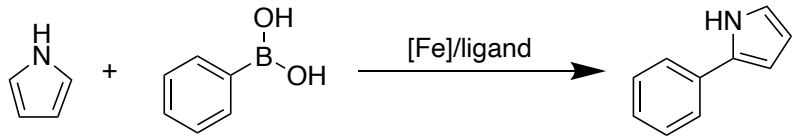

Scheme 3. Iron-ligand mediated coupling of pyrrole and phenylboronic acid to form 2-phenyl pyrrole.

To observe the effects of ligand backbone and substituent electronics on the catalytic yield, iron mediated carbon-carbon catalysis was performed with ligands **L1-L6**. To do this, phenylboronic acid and ligand were added to neat pyrrole (Scheme 3). To this solution was added an iron (III) solution, forming the iron-ligand complex *in situ*. After a twelve-hour reflux, the solution was brought to room temperature and extracted with methylene chloride to remove pyrrole and the polymerized polypyrrole side product. An internal standard of dimethyldiphenylsilane (DMDPS) was added to determine the yield of the reaction via ^{1}H NMR, calculated as shown below.

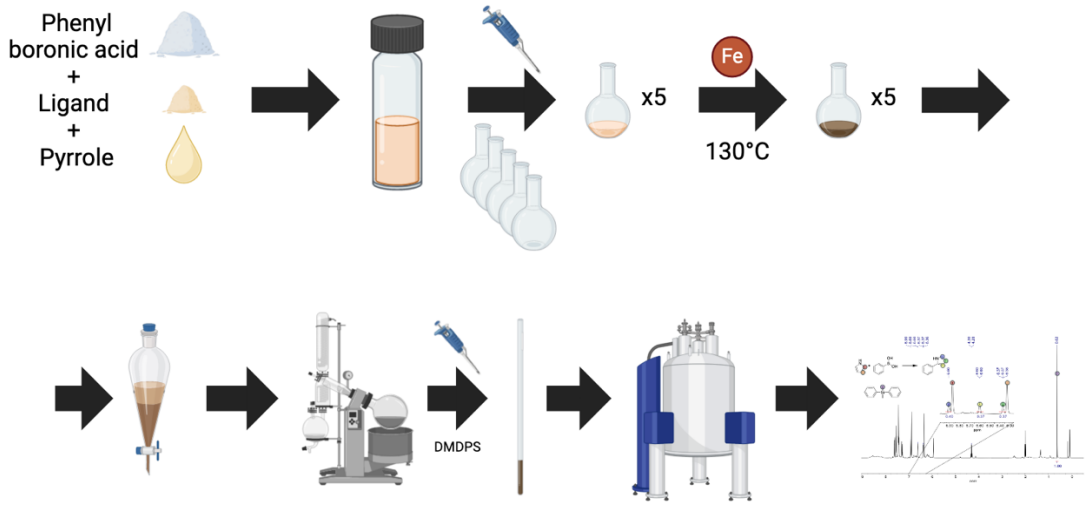

Figure 11. Workflow for C-C catalysis yield determination.

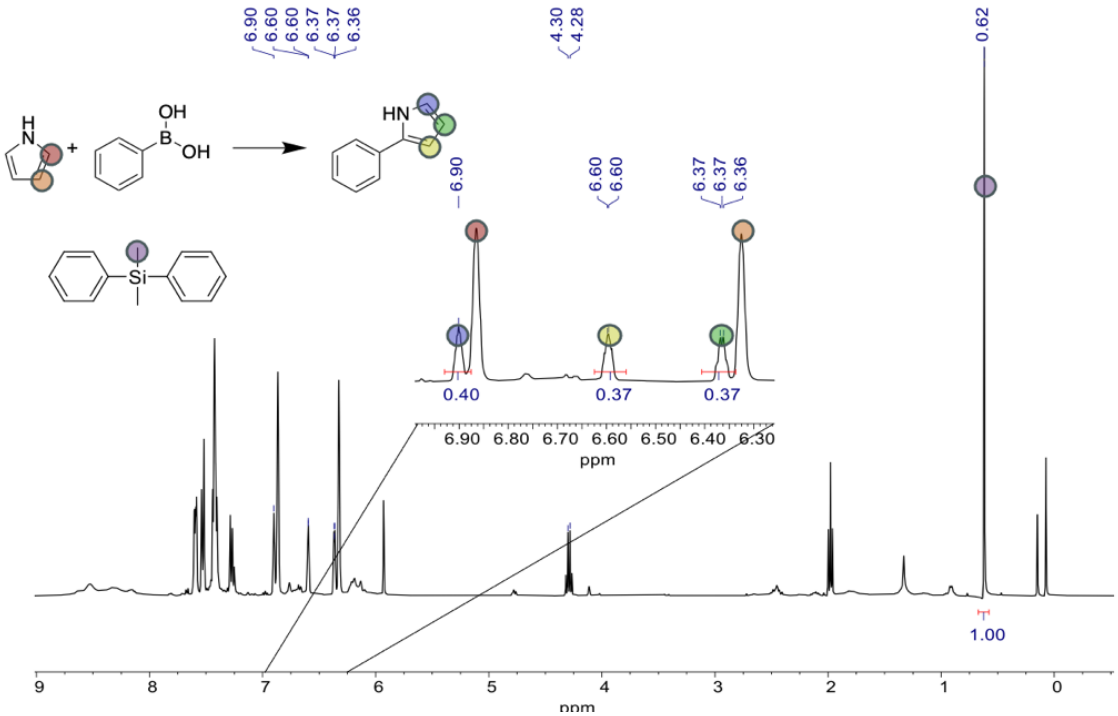

10 μL DMDPS	1 mL	0.985 g DMDPS	1 mol DMDPS	6 mol H	0.37 H	1 mol prod	143.19 g product
	10^3 μL	1 mL DMDPS	212.36 g DMDPS	1 mol DMDPS	1.00 H	H	1 mol product

Figure 12: ^{1}H NMR yield calculations for catalysis.

This reaction was repeated in quadruplet for each ligand **L1-L6**. The comparison of **$^{H}Py_2N_2$** to **$^{H}PyN_3$** (**L3** and **L2**) is shown in Figure 13 to demonstrate the effects of ligand backbone on the catalysis, and the effects of para substitution (**L2-L5**) are shown in Table 1 and Figure 14 below.

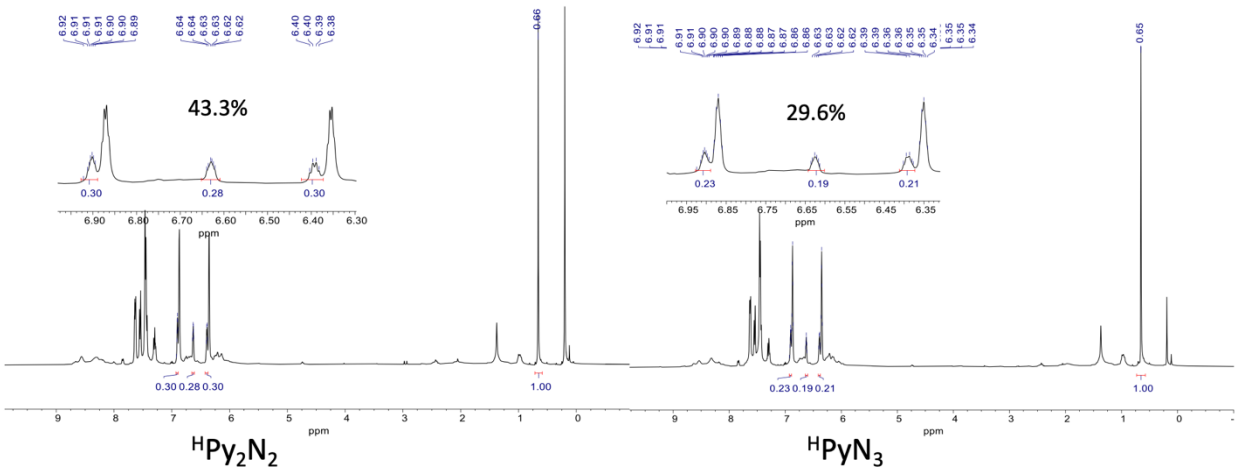

Figure 13. Comparison of PyN_3 and Py_2N_2 backbones as C-C catalysts.

	Hammet Value (para)	Yield (%)	STD
-OMe	-0.27	55	5
-H	0.00	47	3
-Cl	0.23	46	4
-CF3	0.54	65	8

Table 1. Catalytic yield of L2-L5 as a function of Hammet parameter.

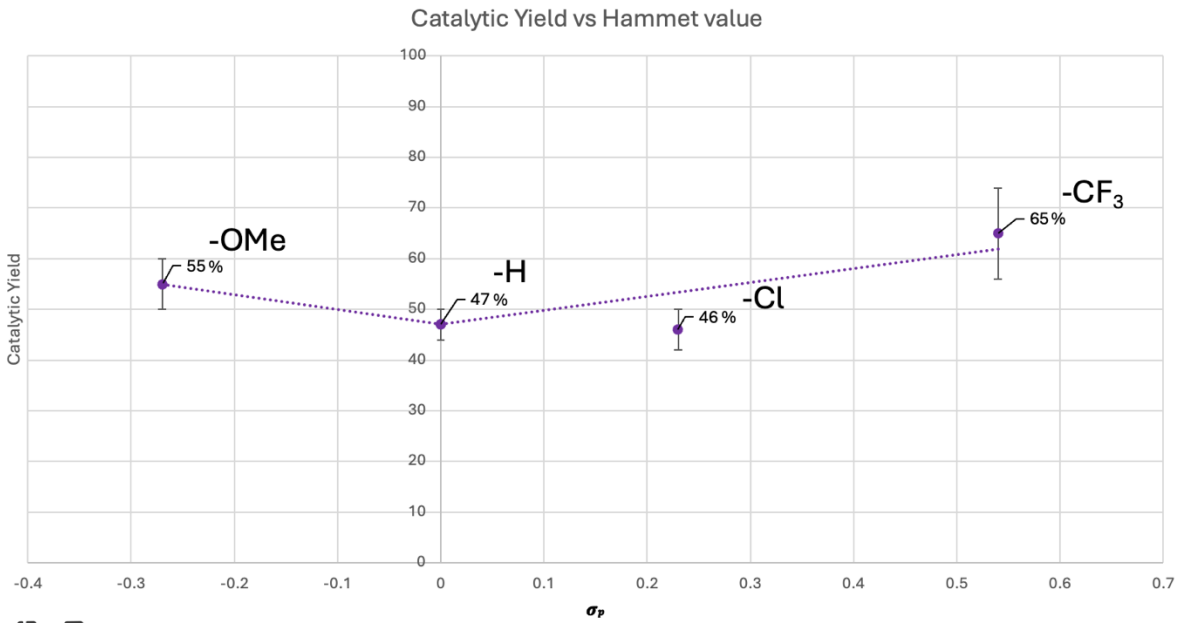

Figure 14. Catalytic Yield of L2-L5 as a function of Hammet parameter.

As the substituent effect ranges from electron-donating to electron-withdrawing, we observe an 'inverted volcano plot,' where both the withdrawing and donating groups increase the yields of the catalysis, with the unsubstituted ligand having the lowest yield.

With the observed yield range of 46-65%, an increase can be seen from that of Mekhail et al.'s range of 32-58%. This can be attributed to the introduction of a second pyridine moiety to the base cyclen structure. Also notable is the comparison of yields achieved by **L5** (^{CF3}**Py$_2$N$_2$**), 65% yield on average, to that of the palladium catalyst $Pd(TFA)_2$, with yields up to 68%. The two are comparable, indicating that the **L5** iron complexes are a competitive catalyst with the currently used palladium ones.

CONCLUSION

With the synthesis and characterization of this $^{R}\mathbf{Py_2N_2}$ series, it has been shown that iron complexes can indeed act as carbon-carbon coupling catalysts at a scale similar to that of the currently used palladium catalysts. When complexed with iron, **L5** was able to catalyze the synthesis of 2-phenyl-pyrrole in yields of 65%, comparable to that of $Pd(TFA)_2$ at 68%.

The findings of contemporary studies such as this provide a foundation for future exploration of iron complexes as palladium catalyst alternatives. Palladium catalysts have been explored for decades, and the scope of their abilities is established. We are in the beginning stages of our understanding of iron catalysts and already seeing promising results. Wen et al. (2010) and the Green Group have explored cyclen derivatives, but other coordinate systems could be explored as catalytic centers. It was found that **L6** was unable to catalyze this reaction due to its iodine moiety causing side reactions; other functional group tolerances should be investigated.

EXPERIMENTAL

I. Experimental notes

Physical Methods and general considerations: The reagents and solvents used in synthesis were obtained from a variety of commercial sources and used as received, unless otherwise noted. All ^{1}H NMR and ^{13}C NMR spectra were acquired through the use of a Bruker Avance III (400 MHz) High Performance Digital NMR spectrometer. Sodium ptoluenesulfonate was synthesized according to a previously published procedure.[16]

II. Synthetic procedures for Ligand L1-L6

Synthesis of L1, L2, L3, L4:

Ligands **L1**, **L2**, **L3**, and **L4** were kindly provided by my colleagues Katie Smith, David Freire, and Sarah Dunn. Methods for synthesis are previously reported.[14,15]

Synthesis of L5 ($^{CF3}Py_2N_2$):

4-Iodo-2,6-bis(carboxymethyl)pyridine (L5.1): A 1000-mL round-bottom flask was charged with **L4.1** (16.01 g, 69.71 mmol), CH_3CN (300 mL), and NaI (104.9 g, 700.0 mmol) and sonicated for 45 minutes at room temperature. Acetyl chloride (16 mL, 224 mmol) was added slowly to the light-yellow suspension, resulting in a dark red color, and the suspension was sonicated for 45 minutes at room temperature. Dichloromethane (200 mL) and sat. Na_2CO_3 (200 mL [to pH=11]) were added, and the solution was transferred to a 1000-mL separatory funnel. The layers were separated, and the aqueous layer was washed with CH_2Cl_2 (200 mL). The organic layers were combined and washed with 150 mL portions of $Na_2S_2O_3$ until the red color faded to light-yellow, sat. NaCl (2 x 100mL) and water (200 mL). The organic phase was dried with anh. Na_2SO_4 and filtered. The solution was concentrated under reduced pressure to give a pale-yellow solid. This was recrystallized in MeOH (500 mL) to give colorless needles (**L5.1**, 21.24 g, 66.17 mmol, 95%). ^{1}H NMR (400 MHz, $CDCl_3$): 8.686 (s, 2H), 4.045 (s, 6H).

4-Carbon-trifluoride-2,6-bis(carboxymethyl)pyridine (L5.2): A 500 mL two-neck flask was charged with **L5.1** (1.41 g, 4.4 mmol), copper (I) iodide (4.99 g, 26.2 mmol), and (dppf)$PdCL_2{\cdot}CH_2CL_2$ (0.18 g, 0.22 mmol). To this was added anh. DMF (70 mL). A solution of methyl 2,2-difluoro-2-(fluorosulfonyl)acetate (5.03 g, 26.2 mmol) in DMF (20 mL) was added to the mixture and allowed to stir at 100 °C under an inert nitrogen atmosphere. After 16 h, the reaction was brought to room temperature, diluted with DCM (50 mL), and filtered through a pad of celite. The filtrate was washed with water (2 x 50 mL) and brine (2 x 75 mL). The organic

phase was dried over Na_2SO_4, filtered, and the solvent was removed by rotovap. The resulting brown oil was subjected to a flash column, using 1:4 ethyl acetate:hexanes and then concentrated under reduced pressure to give a light brown solid (**L5.2**, 1.02 g, 98%). ^{1}H NMR (400 MHz, $CDCl_3$): 8.548 (s, 2H), 4.094 (s, 6H).

4-carbon trifluoride-2,6-bis(hydroxymethyl)pyridine (L5.3): A dry 250 mL two-necked round-bottom flask was charged with **L5.2** (3.00 g, 11.4 mmol), $CaCl_2$ (1.26 g, 11.4 mmol), and anh. MeOH (150 mL) and placed under an N_2 atmosphere. $NaBH_4$ (0.9 g, 22.8 mmol) was added portion-wise at 0 ˚C and stirred vigorously. During the addition, the color changed from an opaque white to a bright orange. After complete addition of $NaBH_4$, the reaction was allowed to stir at room temperature 5 h. The pale yellowish-white solution was filtered through a pad of silica. The silica was washed with copious MeOH and was concentrated under reduced pressure to give a light yellow/orange solid. The solid was dissolved in DI water and basified with NaOH to pH = 9. The product was extracted with ethyl acetate. The organic layer was dried with Na_2SO_4, filtered, and the solvent was removed by rotary evaporation to yield a solid. The product was dried under vacuum overnight, yielding a light brown solid (**L5.3,** 1.35 g, 57%). ^{1}H NMR (400 MHz, DMSO): 7.508 (s, 2H), 4.894 (d, 4H), 3.052 (t, 2H).

4-carbon trifluoride-2,6-bis(p-tosyloxymethyl)pyridine (L5.4): A 250 mL round-bottom flask was charged with **L5.3** (1.23 g, 5.90 mmol) and DCM (50 mL) and then stirred in ice bath until 0°C. A cold KOH solution was added (20 g KOH, 30 g DI H_2O) and stirred. TsCl (2.36 g, 12.4 mmol) was added in one portion. The reaction was stirred at 0°C for 4 h. The solution was transferred to a 250 mL separatory flask, and the organic layer was collected. The aqueous layer was extracted with DCM (3 x 50 mL). All the organic layers were combined and washed with water (3 x 50 mL) then brine (1 x 50 mL). The organic phase was dried with anh. Na_2SO_4, filtered, and rotovapped to a white powder. This was washed with ether and dried to yield a tan solid (**L5.4**, 2.10 g, 69%). ^{1}H NMR (400 MHz, $CDCl_3$): 7.826 (d, 4H), 7.476 (s, 2H), 7.364 (d, 4H), 5.147 (s, 4H), 2.468 (s, 6H). ^{13}C NMR (400 MHz, DMSO): 155.47, 145.54, 140.52, 132.47, 130.06, 128.07, 116.87, 70.49, 21.67.

CF_3-Py_2N_2-Ts·HCl (L5.7): A two-necked 1 L round-bottom-flask was charged with TsNHNa (4.50 g, 23.3 mmol), **L5.4** (6.0 g, 11.6 mmol), and CH_3CN (700 mL) under nitrogen atmosphere. The reaction stirred at reflux for 7 d. The solution was cooled to room temperature and concentrated under reduced pressure to give a pinkish yellow solid **(L5.5 + L5.6)**. EtOH (500

mL) was added to the solid, and it was sonicated and/or stirred overnight. The suspension was filtered, and the resulting yellow powder was washed with EtOH (50 mL) and dried. The powder was transferred to a 1L round bottom flask with EtOH (500 mL), and HCl (1 M, 4 mL) was added. The solution was left to stir at room temperature with a septum for 12 h. The suspension was filtered and washed with EtOH (100 mL), and the filtrate was concentrated under reduced pressure to yield a yellow powder (**L5.7**, 1.26 g, 19%). ^{1}H NMR (400 MHz, DMSO): 8.291 (s, 4H), 7.889 (d, 4H), 7.500 (d, 4H), 4.862 (s, 8H), 2.450 (s, 6H). ^{13}C NMR (400 MHz, $CDCl_3$): 143.29, 139.33, 130.25, 129.61, 127.11, 126.32, 119.00, 21.48.

CF_3-Py_2N_2 (L5): A 100 mL round-bottom flask was charged with **L5.7** (1.50 g, 2.19 mmol) and cc. H_2SO_4 (ca. 10 mL). The mixture was stirred at 120°C for 3 h, then removed from heat and allowed to reach room temperature. The solution was slowly added to 50 mL ice cold water and the aqueous layer was washed with diethyl ether. The aqueous layer was made alkaline (pH > 9, pH paper) through the addition of NaOH and was extracted with dichloromethane (3 x 50 mL), dried with sodium sulfate, and concentrated under reduced pressure to yield an off-white powder. (**L5,** 0.577 g, 71%). ^{1}H NMR (400 MHz, $CDCl_3$): 6.78 (s, 4H), 4.06 (s, 8H). ^{13}C NMR (400 MHz, $CDCl_3$): 161.27, 130.17, 127.11, 115.71, 55.78.

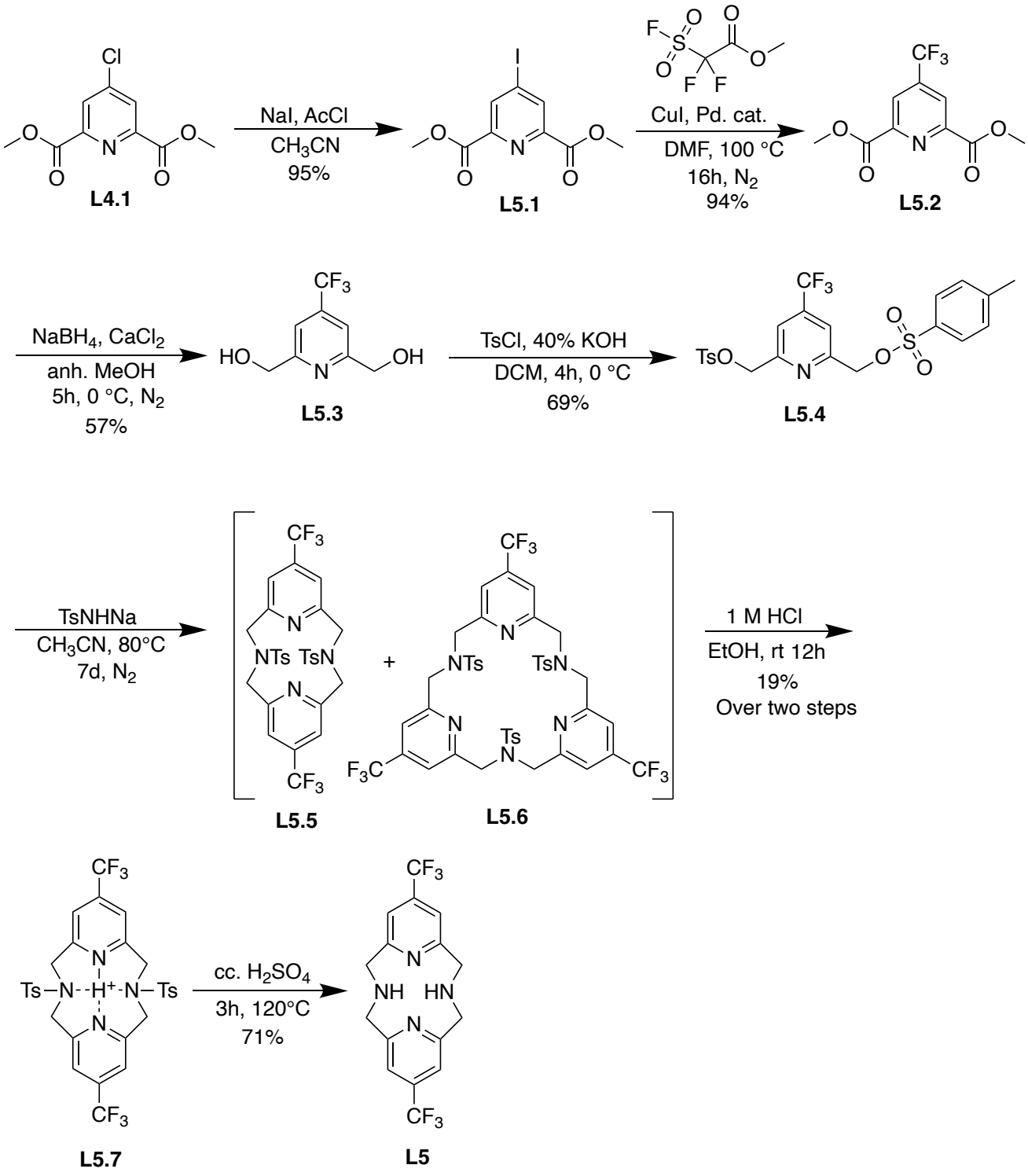

Figure 15. Synthetic Pathway of **L5**.

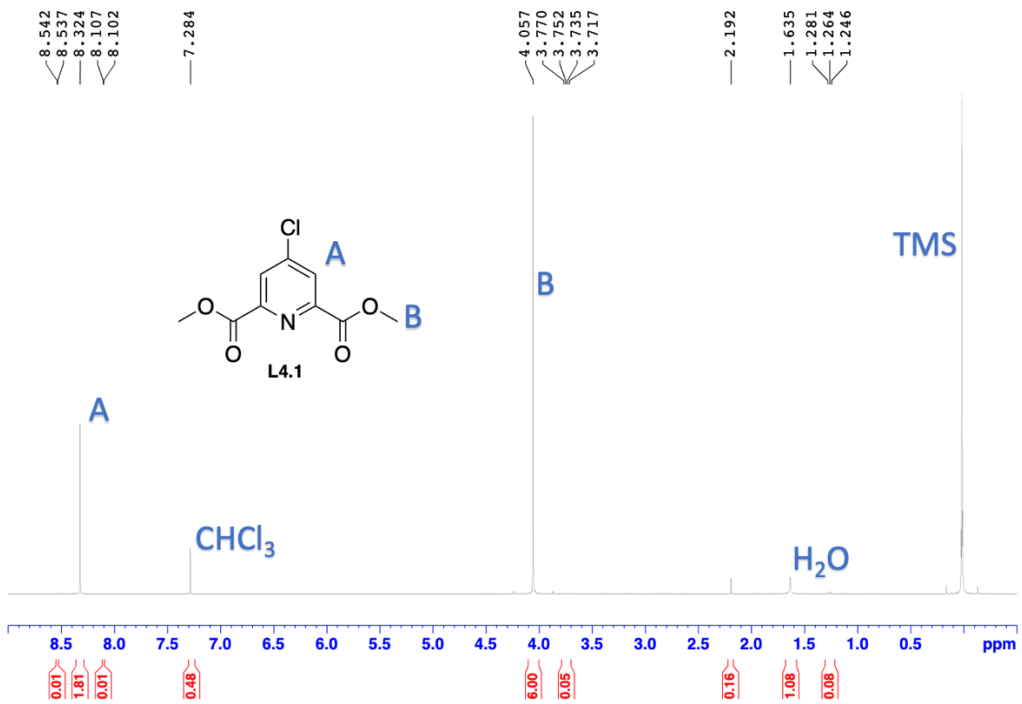

Figure 16. ^{1}H NMR Spectrum of **L4.1** in $CDCl_3$ at 25°C.

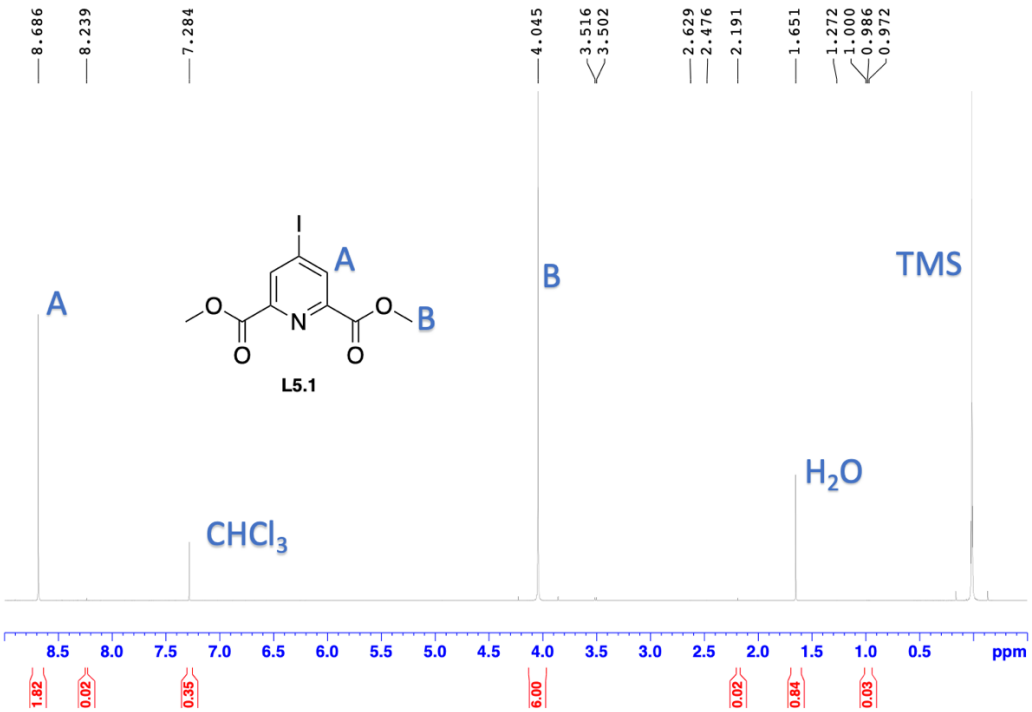

Figure 17. ^{1}H NMR Spectrum of **L5.1** in $CDCl_3$ at 25°C.

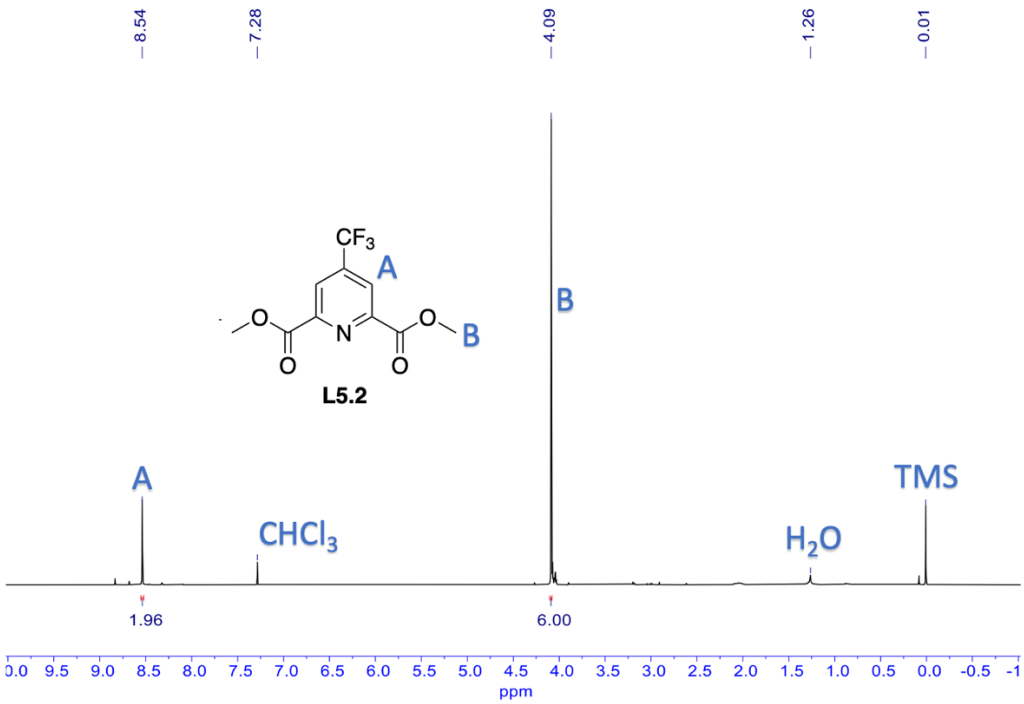

Figure 18. ^{1}H NMR Spectrum of **L5.2** in $CDCl_3$ at 25°C.

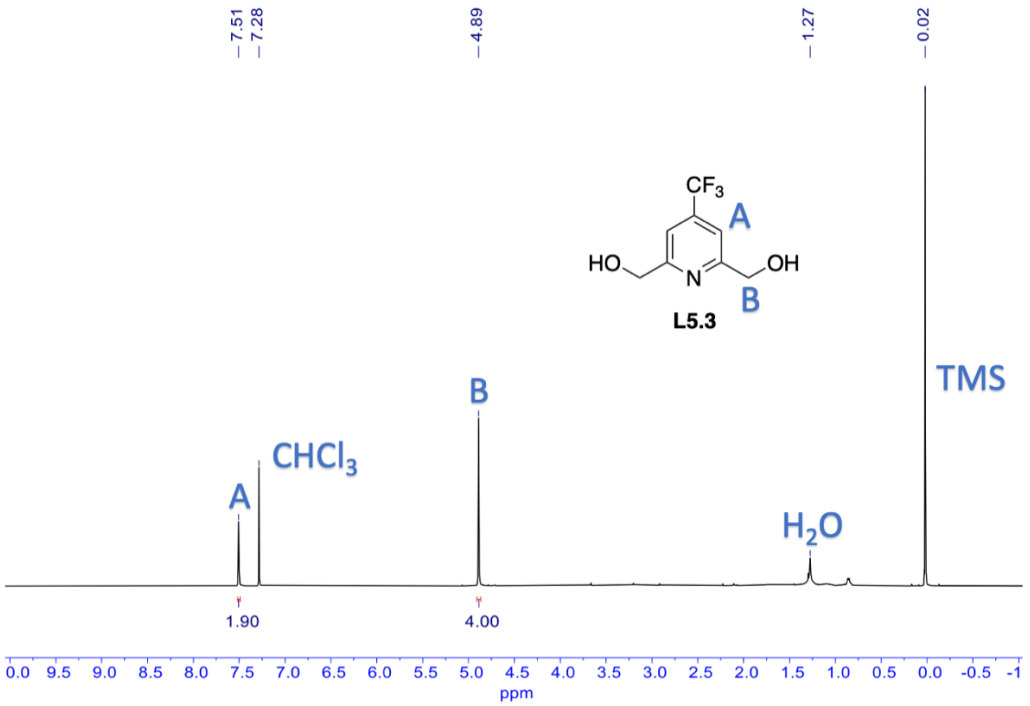

Figure 19. ^{1}H NMR Spectrum of **L5.3** in $CDCl_3$ at 25°C.

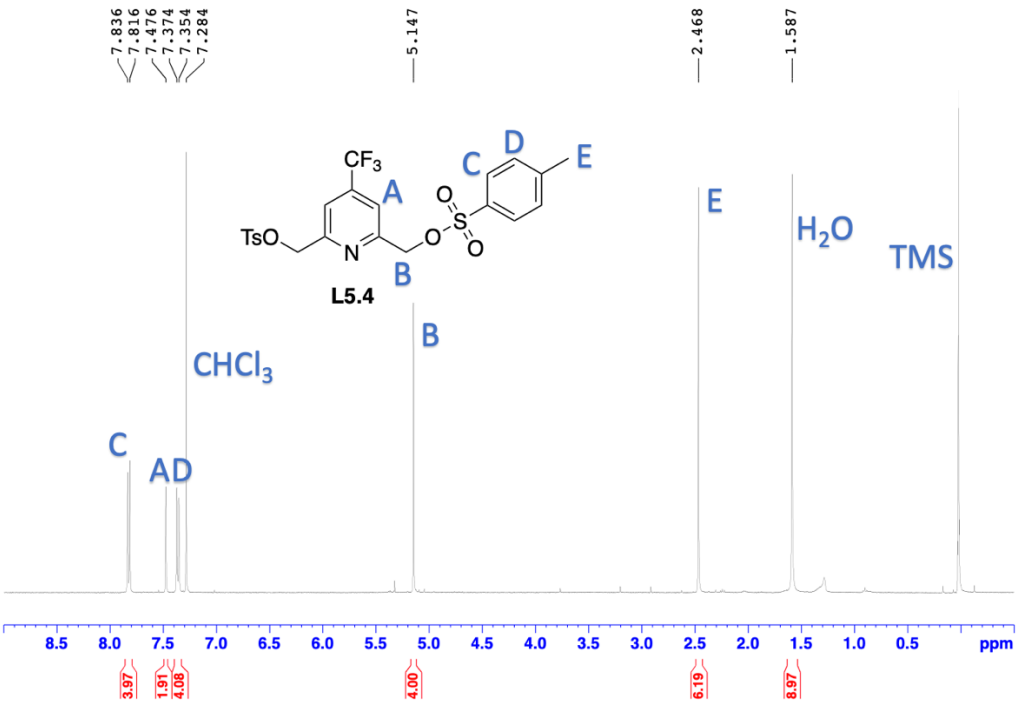

Figure 20. ^{1}H NMR Spectrum of **L5.4** in $CDCl_3$ at 25°C.

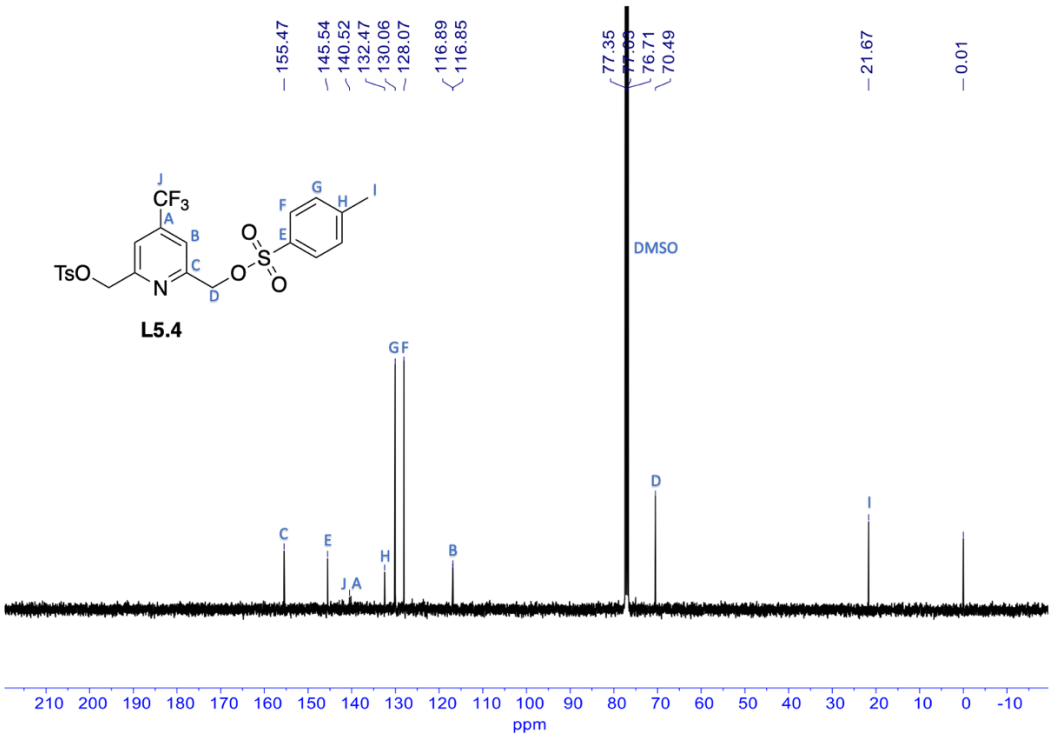

Figure 21. ^{13}C NMR Spectrum of **L5.4** in DMSO at 25°C.

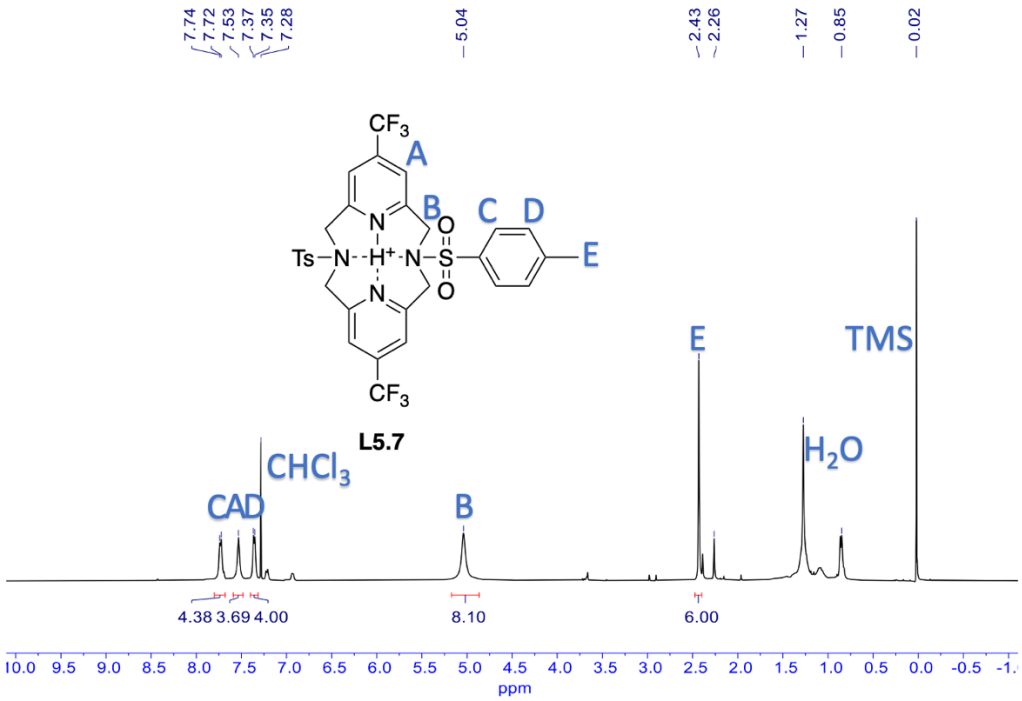

Figure 22. ^{1}H NMR Spectrum of **L5.7** in $CDCl_3$ at 25°C.

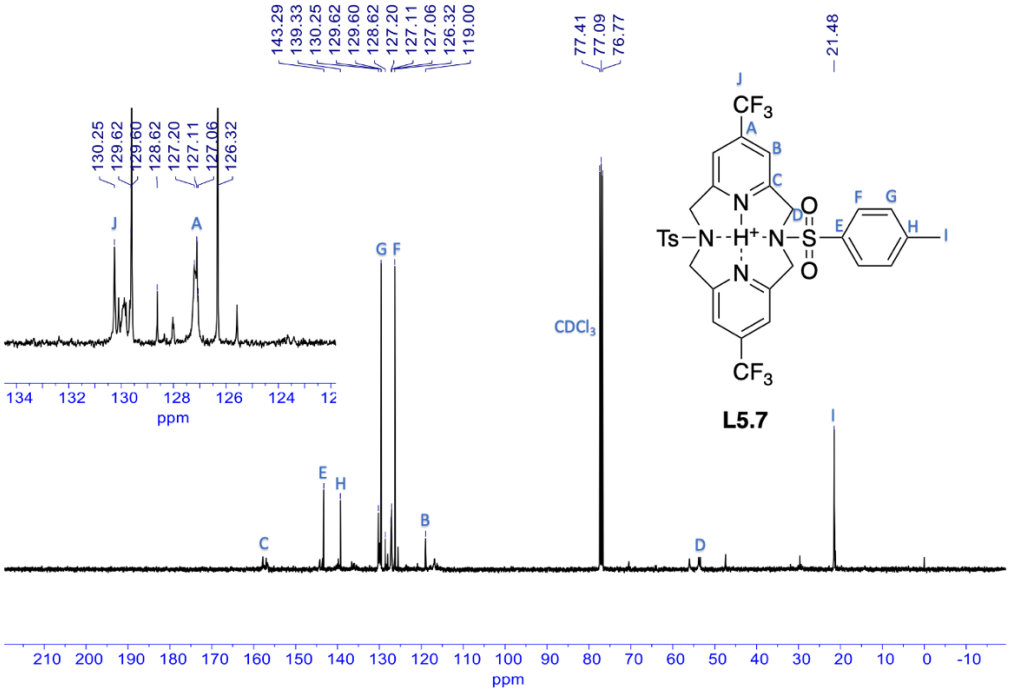

Figure 23. ^{13}C NMR Spectrum of **L5.7** in $CDCl_3$ at 25°C.

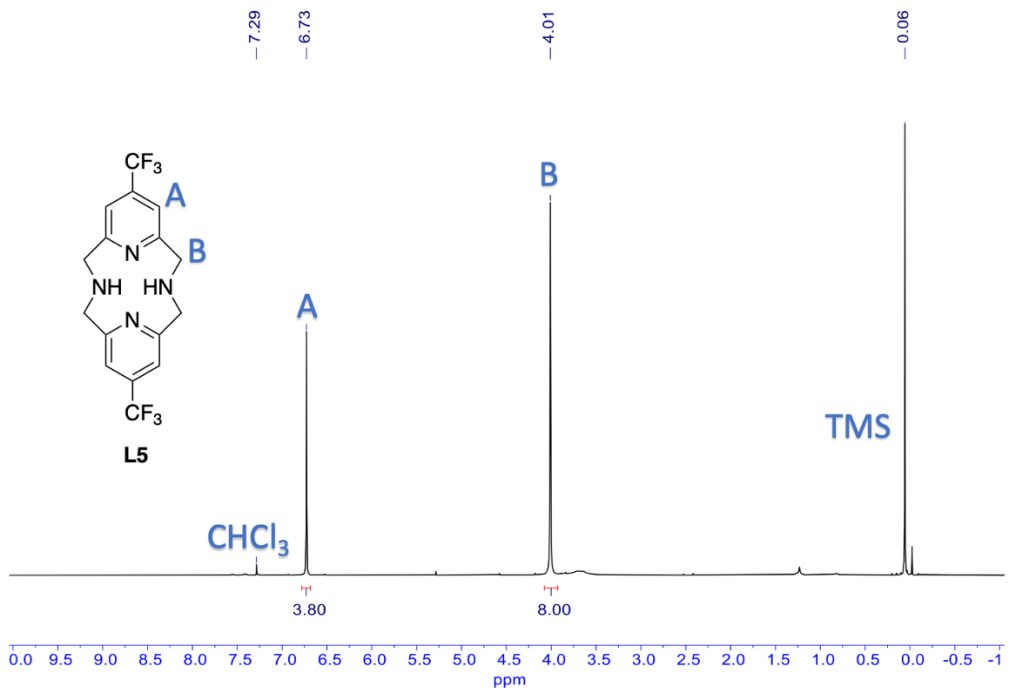

Figure 24. ^{1}H NMR Spectrum of **L5** in $CDCl_3$ at 25°C.

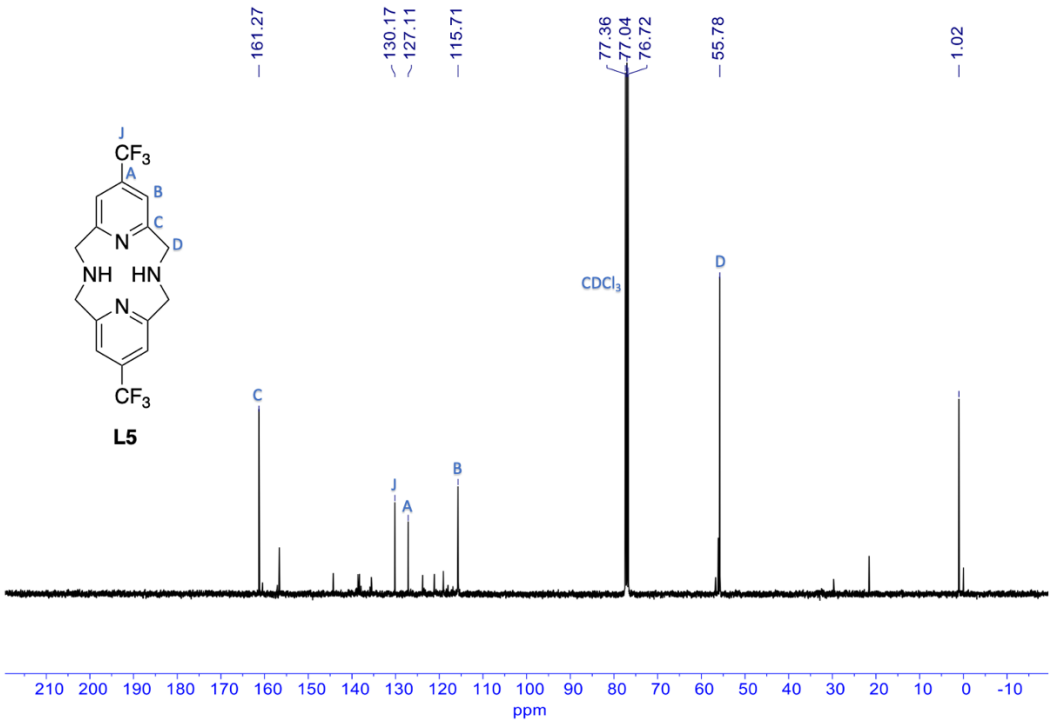

Figure 25. ^{13}C NMR Spectrum of **L5** in $CDCl_3$ at 25°C.

Synthesis of L6 ($^{I}Py_2N_2$):

4-Iodo-2,6-bis(hydroxymethyl)pyridine (L6.1): A dry 250 mL two-necked round-bottom flask was charged with **L5.1** (5.00 g, 15.6 mmol), $CaCl_2$ (1.73 g, 15.6 mmol), and anh. MeOH (150 mL) and placed under an N_2 atmosphere. $NaBH_4$ (1.18 g, 30.1 mmol) was added portion-wise at 0°C and stirred vigorously. During the addition the color changed from an opaque white to a bright orange. After the complete addition of $NaBH_4$, the reaction was allowed to stir at rt 4 h and monitored by TLC [R_f (**SM**)=0.53, R_f (**P**)=0.1] in diethyl ether (Figure 26). The pale yellowish-white solution was filtered through a pad of silica. The silica was washed with copious MeOH and was concentrated under reduced pressure to give a light yellow/orange solid. The solid was dissolved in 50 mL of 1 M HCl and further acidified by addition of cc. HCl until pH=1. Remaining precipitate is removed by filtration. The solution was placed in an ice bath, followed by the addition of 1 M NaOH until a pH of 12. The resulting white precipitate was washed with basified H_2O (150 mL), and the final product was dried under reduced pressure, resulting in a white powder (**L6.1,** 3.39 g, 83%). ^{1}H NMR (400 MHz, DMSO): 7.704 (s, 2H), 5.505 (t, 2H), 4.486 (d, 4H).

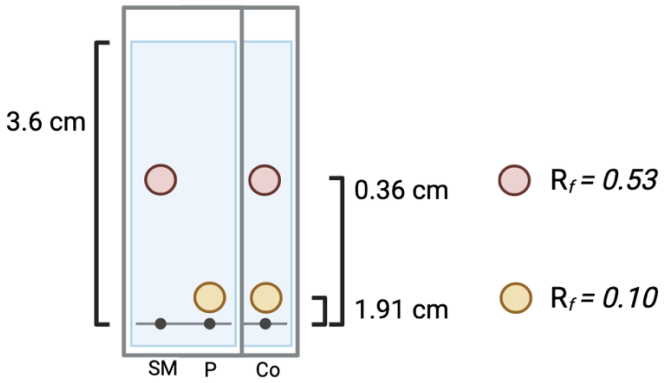

Figure 26. Thin Layer Chromatography of **L6.1** reaction progression.

4-Iodo-2,6-bis(p-tosyloxymethyl)pyridine (L6.2): A 250 mL round-bottom flask was charged with **L6.1** (3.85 g, 14.53 mmol) and DCM (50 mL) and then stirred in ice bath until 0°C. A cold KOH solution was added (20 g KOH, 30 g water) was added and stirred. TsCl (5.92 g, 30.5 mmol) was added in one portion. The reaction was stirred at 0°C for 4 h and monitored by TLC [R_f (**SM**)=0.25, R_f (**P**)=0.75, R_f (**TsCl**)=0.88] in 1:4 hexane:EtOAc (Figure 27). The solution was transferred to a 250 mL separatory flask and the organic layer was collected. The aqueous layer was extracted with DCM (3 x 50 mL). All the organic layers were combined and washed with water (3x 50 mL) then brine (1 x 50 mL). The organic phase was dried with anh. Na_2SO_4,

filtered, and rotovapped to a white powder. This was washed with ether and dried to yield a white powder (**L6.2,** 5.13 g, 62%). ^{1}H NMR (400 MHz, $CDCl_3$): 7.812 (d, 4H), 7.637 (s, 2H), 7.363 (d, 4H), 5.012 (s, 4H), 2.474 (s, 6H). ^{13}C NMR (400 MHz, DMSO): 154.15, 145.66, 138.02, 132.77, 131.77, 130.70, 128.51, 125.96, 71.49, 21.26.

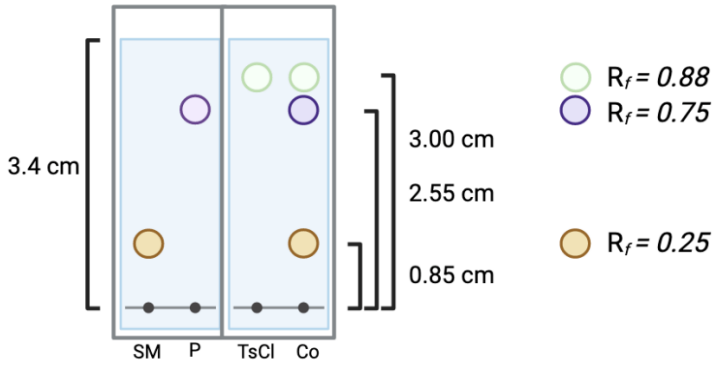

Figure 27. Thin Layer Chromatography of **L6.2** reaction progression.

I-Py$_2$N$_2$-Ts·HCl (L6.5): A two-necked 1 L round-bottom flask was charged with TsNHNa (1.91 g, 9.90 mmol), **L6.2** (2.84 g, 4.95 mmol), and CH_3CN (600 mL) under nitrogen atmosphere. The reaction stirred at reflux for 7 d. The solution was cooled to room temperature and concentrated under reduced pressure to give a pink-yellow solid **(L6.3 + L6.4)**. EtOH (500 mL) was added to the solid, and it was sonicated and/or stirred overnight. The suspension was filtered, and the resulting yellow powder was washed with EtOH (50 mL) and dried. The powder was transferred to a 1L round-bottom flask with EtOH (500 mL) and HCl (1M, 4 mL) was added. The solution was left to stir at room temperature with a septum for 12 h. The suspension was filtered and washed with EtOH (100 mL), and the filtrate was concentrated under reduced pressure to yield a yellow powder (**L6.5,** 0.568 g, 30%). ^{1}H NMR (400 MHz, DMSO): 8.291 (s, 4H), 7.889 (d, 4H), 7.500 (d, 4H), 4.862 (s, 8H), 2.450 (s, 6H).

I-Py$_2$N$_2$ (L6): A 100 mL round-bottom flask was charged with **L6.5** (1.263 g, 1.509 mmol) and cc. H_2SO_4 (ca. 5 mL). The mixture was stirred at 120°C for 3 h, then removed from heat and allowed to reach room temperature. The solution was slowly added to 50 mL ice-cold water and basified with conc. KOH. The solution was concentrated under reduced pressure, resulting in a brown solid. This was suspended in 500 mL $CHCl_3$ and stirred 1 h, filtered, and concentrated under reduced pressure to give a white powder (**L6,** 0.536 g, 72.2%). ^{1}H NMR (400 MHz, $CDCl_3$): 7.02 (s, 4H), 3.88 (s, 8H).

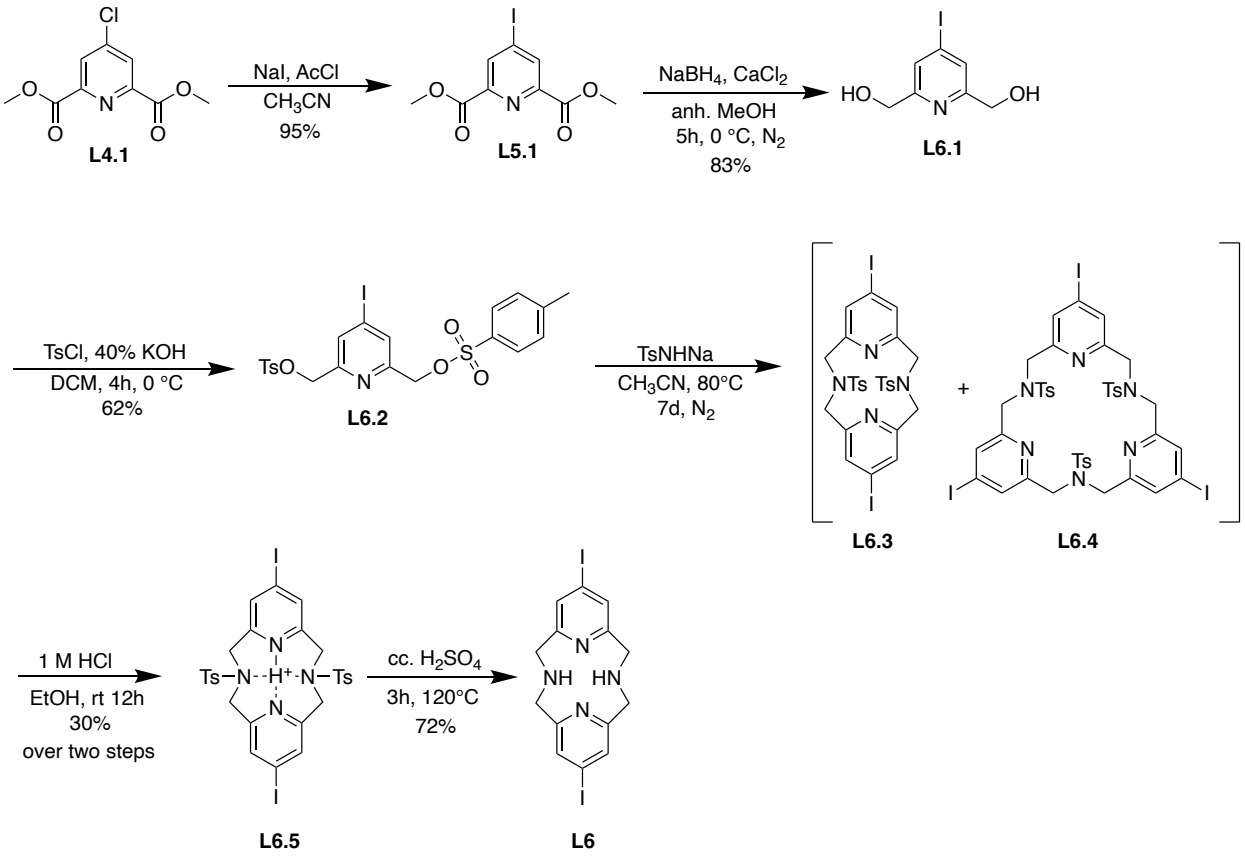

Figure 28. Synthetic Pathway of **L6**.

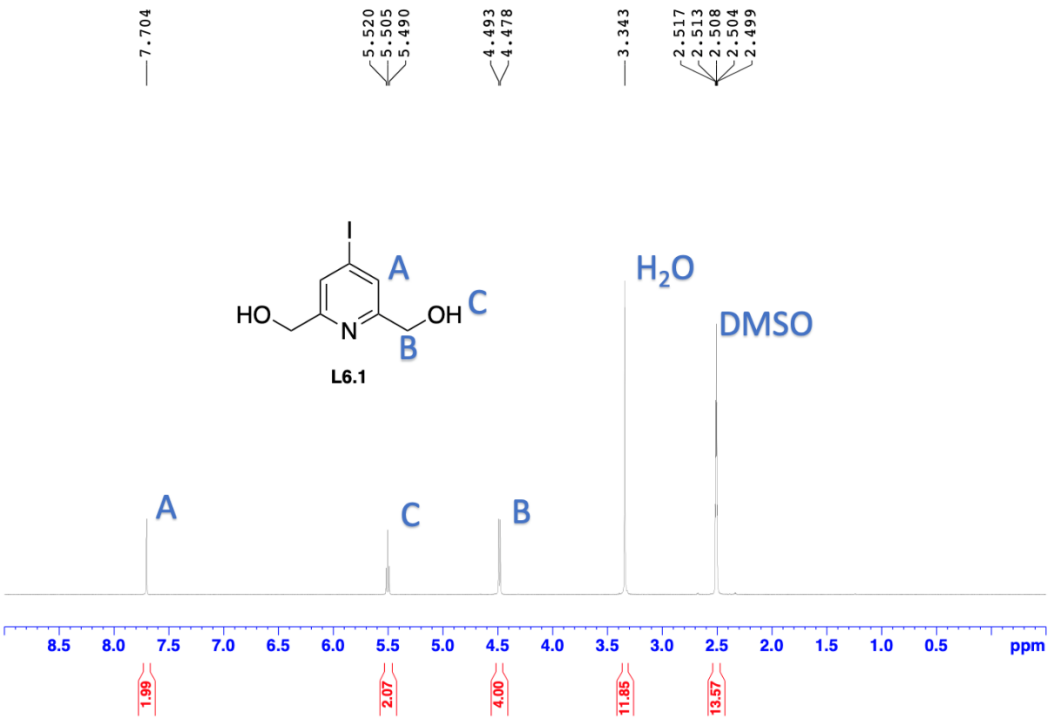

Figure 29. ^{1}H NMR Spectrum of **L6.1** in DMSO at 25°C.

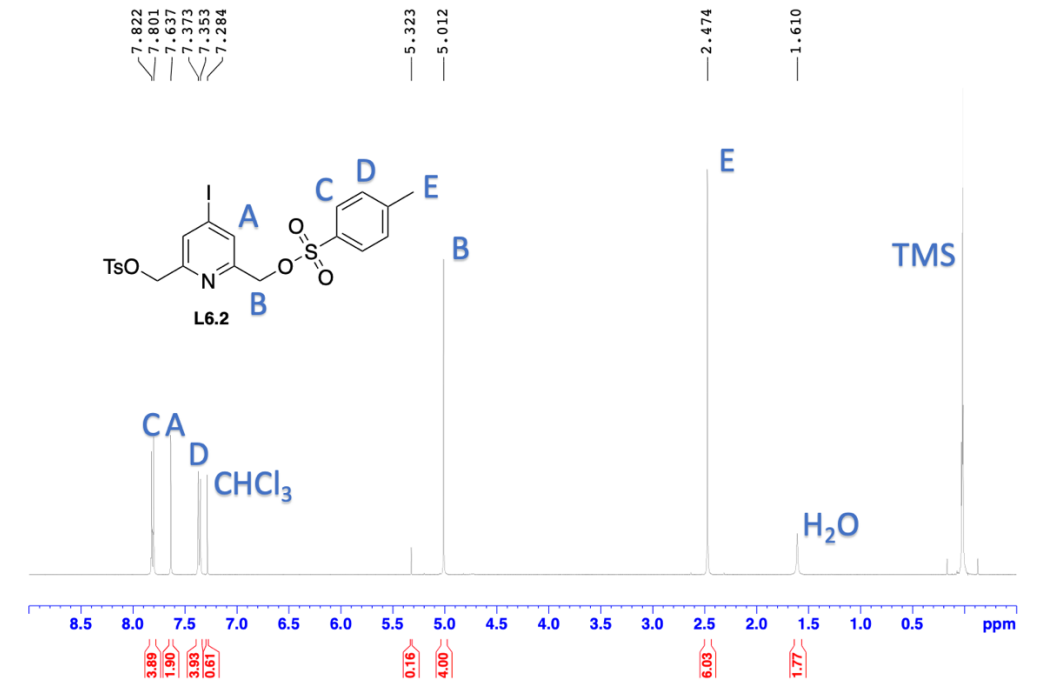

Figure 30. ^{1}H NMR Spectrum of **L6.2** in $CDCl_3$ at 25°C.

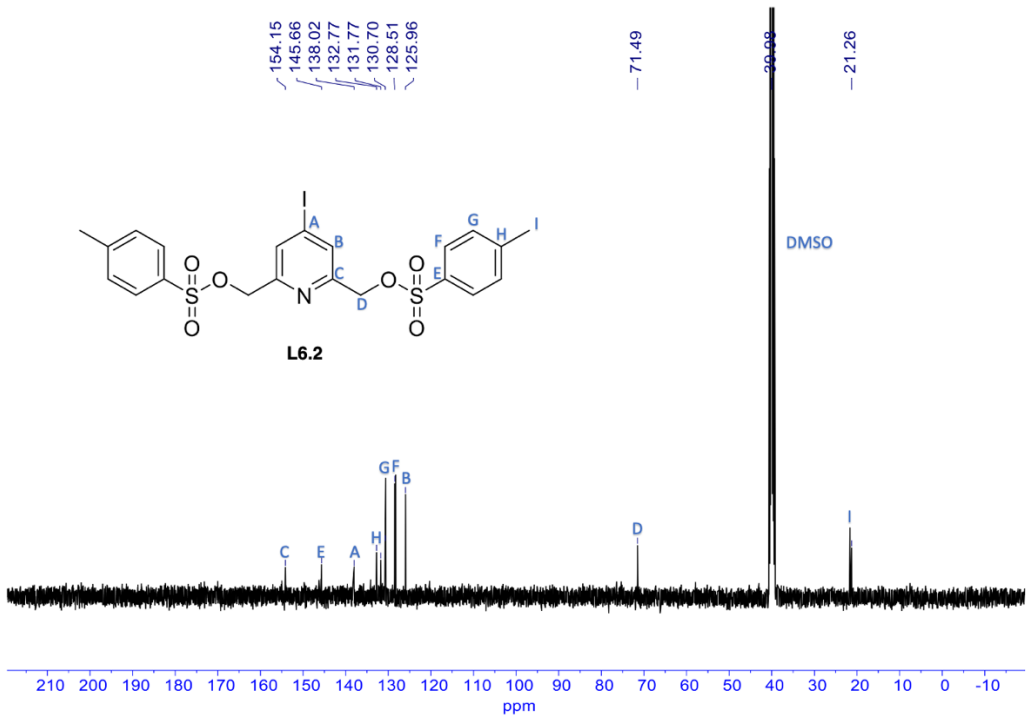

Figure 31. ^{13}C NMR Spectrum of **L6.2** in DMSO at 25°C.

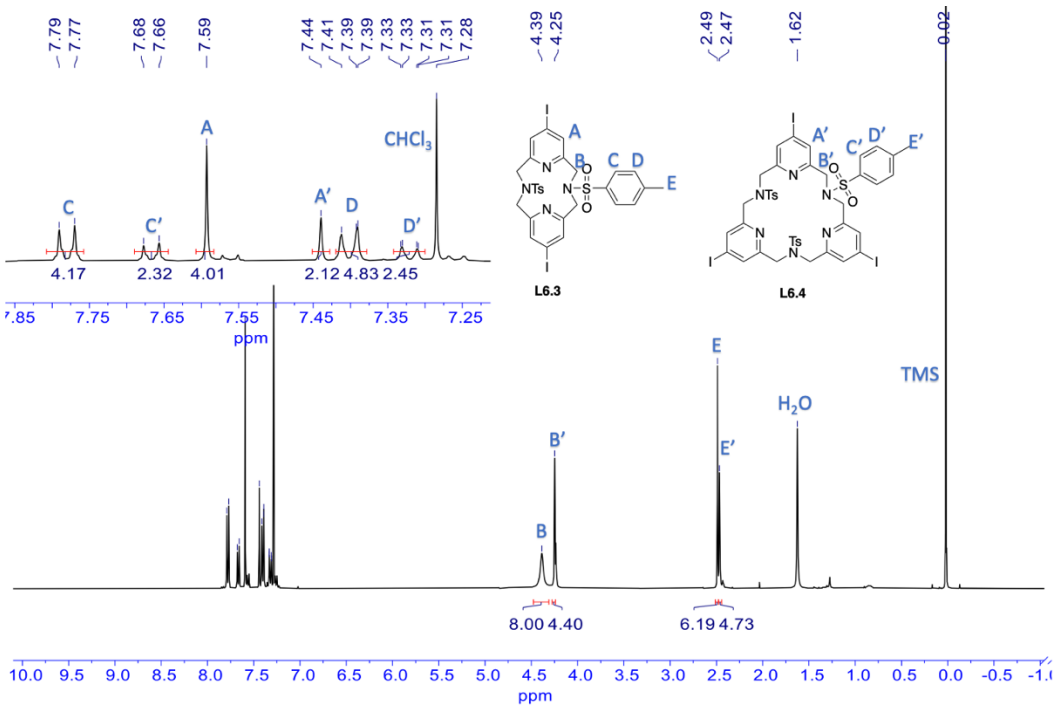

Figure 32: ^{1}H NMR Spectrum of **L6.3 + L6.4** (dimer trimer mix) in $CDCl_3$ at 25°C.

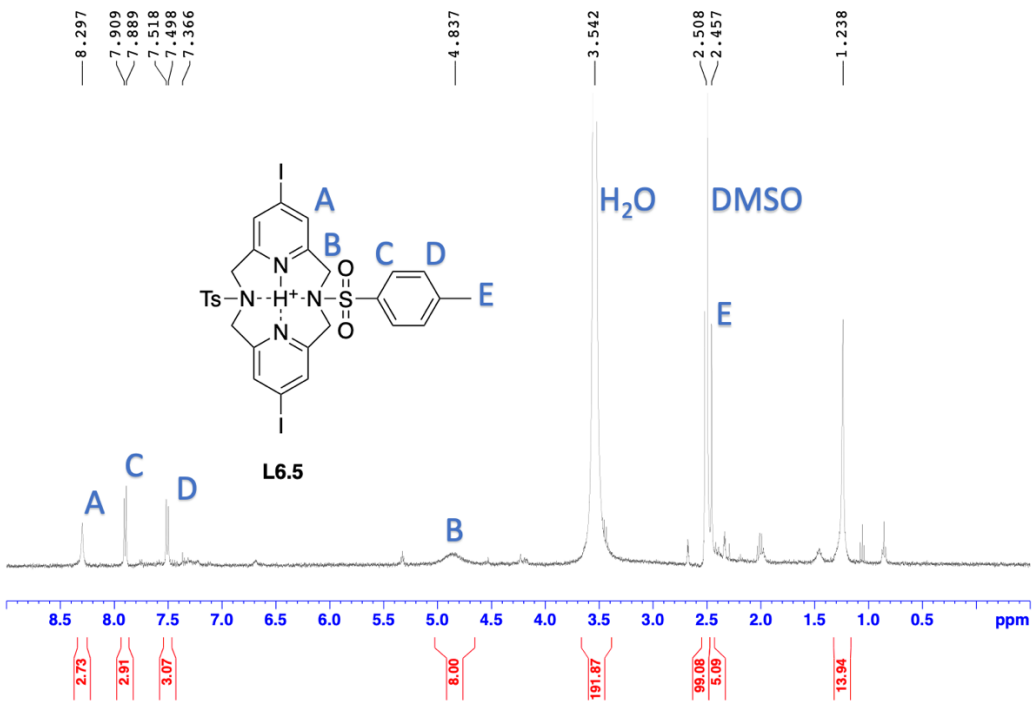

Figure 33. ^{1}H NMR Spectrum of **L6.5** in DMSO at 25 °C.

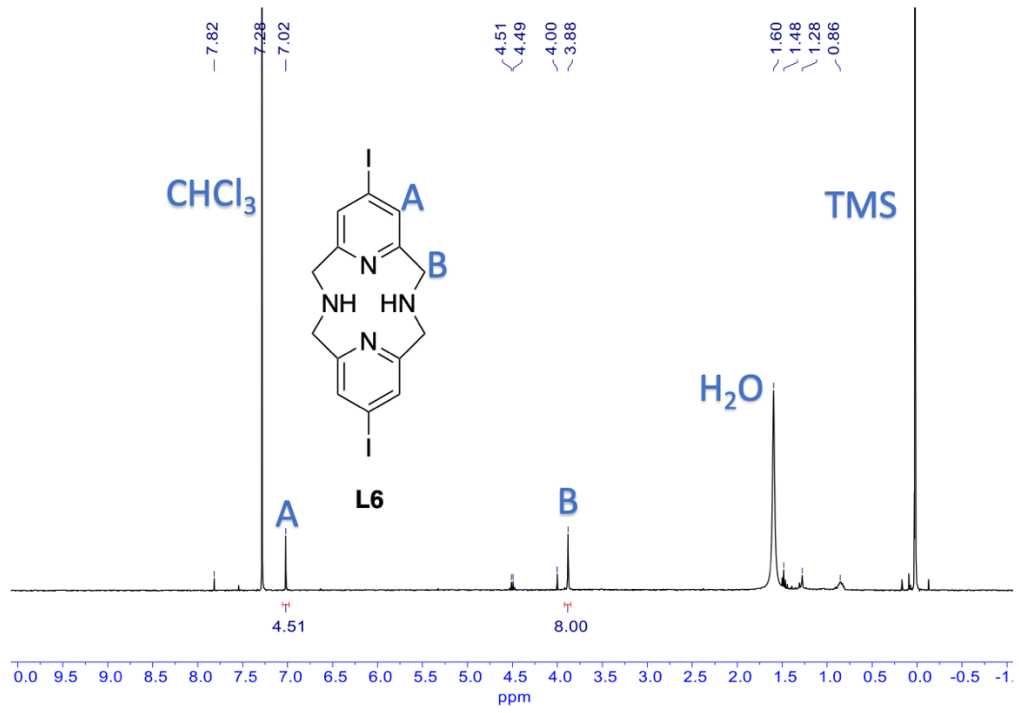

Figure 34. ^{1}H NMR Spectrum of **L6** in $CDCl_3$ at 25 °C.

III. Catalytic Coupling Experimental Procedure:

I. Pre-Reaction Steps:

To ensure the correct catalytic loading of 10% mol, the percent mass composition of crude L1-L5 samples must be determined. This was achieved through the use of an internal ^{1}H NMR standard, sodium trimethylsilylpropanesulfonate (DSS). To do this, three samples were prepared. To the first sample were added no solids. To the second and third was added a known amount of DSS, ca. 5 mg, each. To the third alone was added a known amount of crude ligand ca. 5 mg. Three 750 µL ampules of d6-DMSO were combined—in order to ensure uniform solvent wetness—and a 700 µL aliquot of d6-DMSO was added to each sample. A ^{1}H NMR spectrum was obtained of each sample and the integrations were standardized by setting the DMSO resonance ($\delta \approx 2.5$ ppm) to an integration of 10.000.

An example of these calculations is shown below for L4.

Sample	DMSO-d_6 (µL)	DSS (mg)	**L4** (mg)
I	700	-	-
II	700	4.4	-
III	700	4.6	3.4

Table 2. Sample preparation for ligand percent mass composition determination.

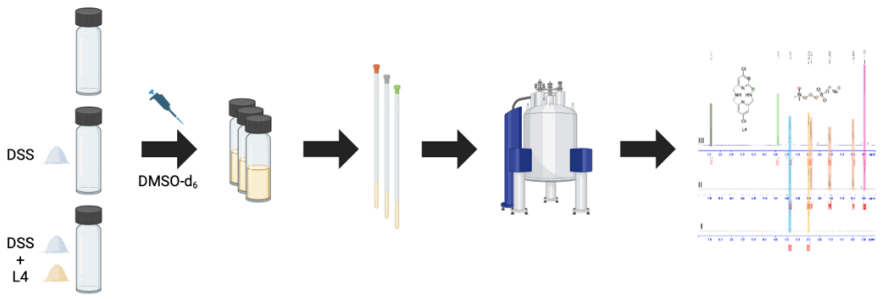

Figure 35. Workflow for sample preparation for ligand percent mass composition determination.

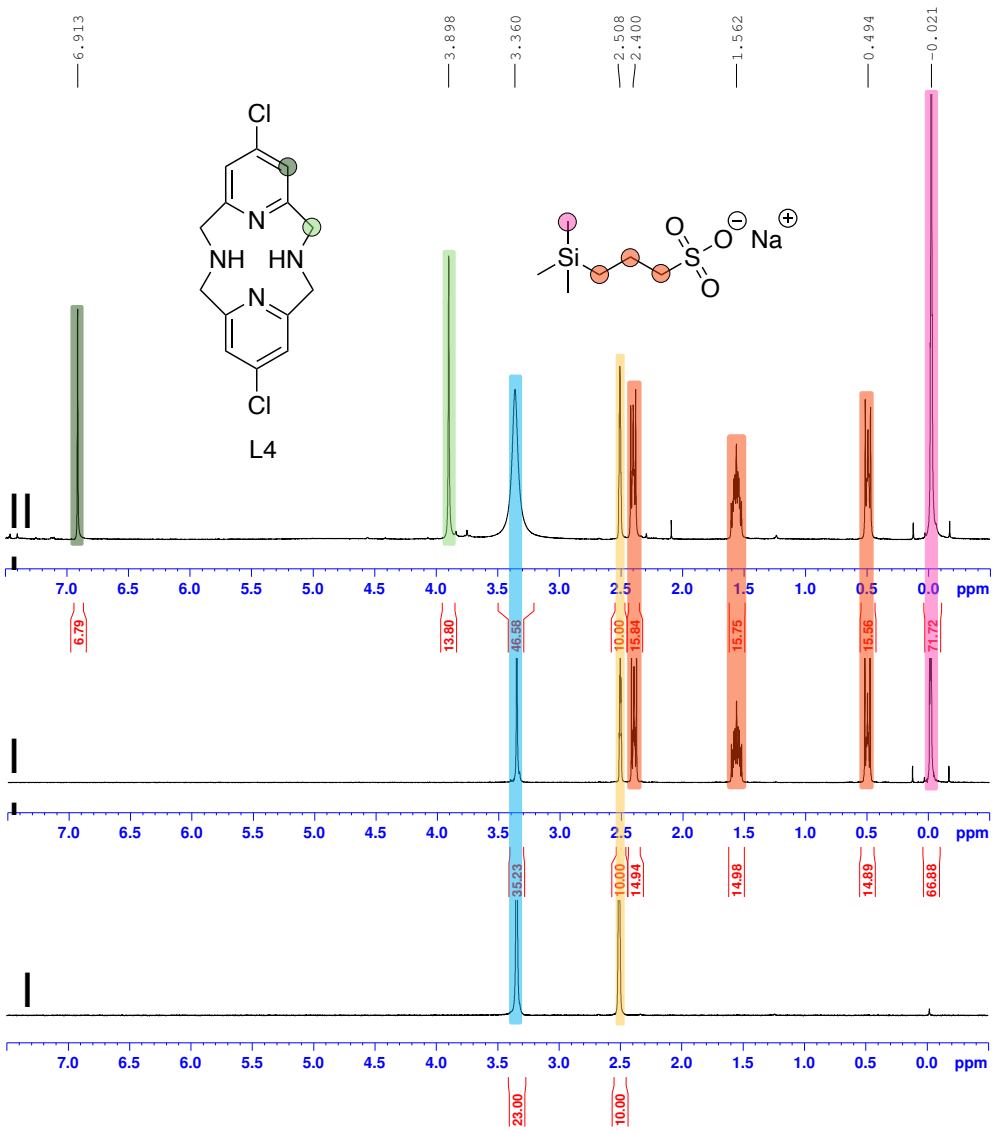

Figure 36. NMR spectra of Samples I, II, III for DSS calculations of **L4**.

By looking at the first spectrum of DMSO-d_6 alone, we can attribute the entirety of water resonance (3.360 ppm) to the wetness of the DMSO-d_6 used. Using this, we can determine the amount of the water integration that can be attributed to the DSS in the second sample by subtracting the two.

$$int_{2,H_2O} - int_{1,H_2O} = int_{DSS,H_2O} \quad (1a)$$

$$35.23\ int - 23.00\ int = 12.23\ int_{H_2O} \text{ in } 4.4 \text{ mg } DSS_{wet} \quad (1b)$$

The integrations of the second spectrum reveal the ratio between the DSS and the water in the sample. The adjusted 12.23 integration at 3.360 ppm corresponds to the 2 H in water. The 3 integrations at 0.940-2.40 ppm, averaging 14.94 int, correspond to 2 H each in DSS. The molecular weight of 'wet DSS' can be determined through this knowledge.

$$mw_{DSS_{wet}} = \frac{\frac{int_{DSS}}{n\,DSS_H}(mw_{DSS}) + \frac{int_{H_2O}}{n\,H_2O_H}(mw_{H_2O})}{\frac{int_{DSS}}{n\,DSS_H}} \tag{2a}$$

$$mw_{DSS_{wet}} = \frac{\frac{14.94\ int}{2\ H}\left(218.32\frac{g}{mol}\right) + \frac{12.23\ int}{2\ H}\left(18.02\frac{g}{mol}\right)}{\frac{14.94\ int}{2\ H}} = 233.07\,\frac{g}{mol} \tag{2b}$$

With this known molecular weight of the wet DSS, the third spectrum can be used to determine the amount of **L4** present, and by knowing the amount of crude **L4** added we can determine the percent composition of $\mathbf{L4}/\mathbf{L4}_{\text{crude}}$, using the 0.940-2.400 ppm (alkane) integrations of DSS. There are three sets of resonances in this range, each corresponding to 2 H. Taking the average of their integrations, we can assign that average to 2 H and use this as a conversion factor to the 3.898 ppm (corresponding to the CH_2 α to the pyridine) integration of **L4**, representing 8 H.

$$\frac{4.6\ mg\ DSS_{wet}}{3.4\ mg\ L4_{crude}} \times \frac{1\ g}{1000\ mg} \times \frac{1\ mol\ DSS_{wet}}{233.07\ g\ DSS_{wet}} \times \frac{1\ mol\ DSS}{1\ mol\ DSS_{wet}} \times \frac{2\ H}{1\ mol\ DSS} \times \frac{13.80\ H}{15.72\ H} \times \frac{1\ mol\ L4}{8\ H} \times \frac{309.19\ g\ L4}{1\ mol\ L4} \times \frac{1000\ mg}{1\ g} \times 100\% = 39.3\%\ \boldsymbol{L4}/L4_{crude} \tag{3}$$

With this percent composition known, we can ensure the correct amount of $\mathbf{L4}_{\text{crude}}$ is added to the reaction flask. When running the experiment in quadruplicate, 4.2 times the amount of all reagents are added. For **L4**, this looks like:

$$4.2\ trials \times \frac{0.01968\ mmol\ L4}{1\ trial} \times \frac{309.19\ mg\ L4}{1\ mmol\ L4} \times \frac{100\ mg\ L4_{crude}}{39.3\ mg\ L4} = 65.0\ mg\ L4_{crude} \tag{4}$$

II. Catalysis:

To a clean vessel was added ligand (82.7 µmol), phenylboronic acid (827 µmol, 100.8 mg), and 4.2 mL of pyrrole. This solution was sonicated to ensure dissolution. Aliquots (1 mL) of this solution were added to four dry 10 mL round bottom flasks, each wrapped in aluminum foil. To each flask was added 9.9 µL of a 0.9 mg/µL iron (III) trifluoromethanesulfonate solution. These were allowed to reflux at 130°C for 12 h

exposed to the atmosphere. The flasks were then allowed to come to room temperature and were worked up individually. The solutions were transferred to a separatory funnel with chloroform (50 mL) and water (50 mL). The aqueous layer was extracted with chloroform (2 x 50 mL). The combined organic layers were washed with water (50 mL) and brine (50 mL), dried over Na_2SO_4, and filtered. The resulting solution was concentrated under reduced pressure and left to dry further overnight. To the sample was added 700 μL of $CDCl_3$ and 10 μL of dimethyldiphenylsilane, used to determine the yield as shown in Figure 12. ^1H NMR (400 MHz, $CDCl_3$): 6.900 (s, 1H), 6.600 (s, 1H), 6.370 (s, 1H).

REFERENCES

1. Smokefoot. CatalysisScheme. https://en.m.wikipedia.org/wiki/File:CatalysisScheme.png (accessed 2024-05-06).
2. Green, K. N. Collaborative Research: Establishing Earth Abundant Iron/Tetra-Aza Macrocyclic Complexes to Mediate Direct Arylation of Un-Activated Arenes. *NSF Grant Proposal* **2023**.
3. heisenberg.chem. *Instagram*. 2021.
4. Pagett, A. B.; Lloyd-Jones, G. C. Organic Reactions. *Organic Reactions* **2020**, *100*, 547–619. DOI:10.1002/0471264180.
5. VOA News. Protest Follows Firing of 12,000 South African Miners. https://www.voanews.com/a/protest-follows-firing-of-south-african-minors/1521602.html (accessed 2024-05-06).
6. Levelle, M. How Norilsk, in the Russian Arctic, Became One of the Most Polluted Places on Earth. https://www.nbcnews.com/news/world/norilsk-russian-arctic-became-one-polluted-places-earth-rcna6481 (accessed 2024-05-06).
7. Nuss, P.; Eckelman, M. J. Life Cycle Assessment of Metals: A Scientific Synthesis. *PLoS ONE* **2014**, *9* (7). DOI:10.1371/journal.pone.0101298.
8. Chirik, P. J.; Engle, K. M.; Simmons, E. M.; Wisniewski, S. R. Collaboration as a Key to Advance Capabilities for Earth-Abundant Metal Catalysis. *Organic Process Research & Development* **2023**, *27* (7), 1160–1184. DOI:10.1021/acs.oprd.3c00025.
9. Berger, O.; Winters, K. R.; Sabourin, A.; Dzyuba, S. V.; Montchamp, J.-L. On the Cost of Academic Methodologies. *Organic Chemistry Frontiers* **2019**, *6* (12), 2095–2108. DOI:10.1039/c9q00020f.
10. Bertini, I.; Gray, H. B.; Stiefel, E. I.; Valentine, J. S. *Biological Inorganic Chemistry: Structure & Reactivity*; University Science Books, 2007.
11. Choy, P. Y.; Wong, S. M.; Kapdi, A.; Kwong, F. Y. Recent Developments in Palladium-Catalysed Non-Directed Coupling of (Hetero)Arene C–H Bonds with C–Z (Z = b, Si, Sn, s, N, C, H) Bonds in Bi(Hetero)Aryl Synthesis. *Organic Chemistry Frontiers* **2018**, *5* (2), 288–321. DOI:10.1039/c7q000693d.
12. Wen, J.; Qin, S.; Ma, L.-F.; Dong, L.; Zhang, J.; Liu, S.-S.; Duan, Y.-S.; Chen, S.-Y.; Hu, C.-W.; Yu, X.-Q. Iron-Mediated Direct Suzuki–miyaura Reaction: A New Method for the *Ortho*-Arylation of Pyrrole and Pyridine. *Organic Letters* **2010**, *12* (12), 2694–2697. DOI:10.1021/ol100838m.
13. Mekhail, M. A.; Pota, K.; Kharel, S.; Freire, D. M.; Green, K. N. Pyridine Modifications Regulate the Electronics and Reactivity of Fe–Pyridinophane Complexes. *Dalton Transactions* **2022**, *52* (4), 892–901. DOI:10.1039/d2dt03485a.
14. Mekhail, M. A.; Smith, K. J.; Freire, D. M.; Pota, K.; Nguyen, N.; Burnett, M. E.; Green, K. N. Increased Efficiency of a Functional Sod Mimic Achieved with Pyridine Modification on a Pyclen-Based Copper(Ii) Complex. *Inorg. Chem.* **2023**, *62* (14), 5415–5425. DOI:10.1021/acs.inorgchem.2c04327.
15. Yepremyan, A.; Mekhail, M. A.; Niebuhr, B. P.; Pota, K.; Sadagopan, N.; Schwartz, T. M.; Green, K. N. Synthesis of 12-Membered Tetra-Aza Macrocyclic Pyridinophanes Bearing

Electron-Withdrawing Groups. *J. Org. Chem.* **2020**, *85* (7), 4988–4998. DOI:10.1021/acs.joc.0c00188.

16. Bottino, F.; Di Grazia, M.; Finocchiaro, P.; Fronczek, F. R.; Mamo, A.; Pappalardo, S. Reaction of Tosylamide Monosodium Salt with Bis(Halomethyl) Compounds: An Easy Entry to Symmetrical N-Tosyl Aza Macrocycles. *J. Org. Chem.* **1988**, *53* (15), 3521–3529. DOI:10.1021/jo00250a020.